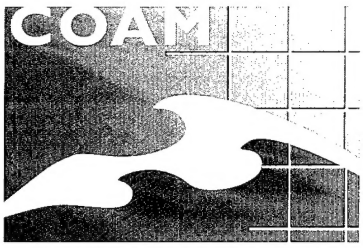

Center for
Ocean/Atmospheric
Modeling

Building 1103
Stennis Space Center
Mississippi 39529

Phone 601-688-5737
FAX 601-688-7072

COUPLING A BASIN-WIDE, COARSE-RESOLUTION NORTH ATLANTIC AND A REGIONAL, FINE-RESOLUTION GULF OF MEXICO MODEL

Germana Peggion

The University of
Southern Mississippi

TR-1/96

October 1995

The Center for Ocean & Atmospheric Modeling (COAM) is operated by The University of Southern Mississippi under sponsorship of the Department of the Navy, Office of the Chief of Naval Research. Any opinions, findings, and conclusions or recommendations expressed in this publication are those of the author and do not necessarily reflect the position or the policy of the U.S. Government, and no official endorsement should be inferred.

ABSTRACT

A reduced-gravity model is configured in the North Atlantic (NAtl) Ocean and Gulf of Mexico (GOM) to investigate the wind-driven circulation and the variability of the associated current systems. The analysis is focused on the circulation of the western tropical NAtl and its relationship to the mesoscale activity inside the GOM. Several experiments investigate the solutions as a function of the Rossby radius of deformation and the specification of the South Atlantic inflow. The GOM dynamics are analyzed with both the basin-wide coarse-resolution and the regional high-resolution models. Both configurations are able to reproduce eddy shedding: the time and length scales of the Loop Current (LpCur) variability do not depend upon the grid resolution. The NAtl simulations indicate that the transport at the Yucatan and Florida Straits are not strongly correlated. Also, no significant correlation is found between eddy shedding events and the GOM transport anomaly.

The evolution of the LpCur instability is dependent upon the Rossby radius of deformation, L_R, rather than inflow transport. For large L_R, the separated rings migrate westward as dispersive linear Rossby waves. As L_R decreases, the detached eddies migrate as nonlinear, isolated vortices. The nonlinear character of the LpCur increases with the inflow transport and enhances more interaction between rings and the main stream during separation events.

1. INTRODUCTION

The implementation of a numerical model requires a set of designing choices involving the physics to be reproduced and the mathematical and numerical formulation of the dominant dynamical processes. Computational considerations have usually been the major constraint in modeling the ocean. In general, the models which are the most dynamically simple are the most computationally efficient. As the main memory of computers is expanded and computing power is increased, it becomes possible to apply full 3-D, primitive equation models to basin-wide domains and describe and reproduce the mesoscale variability of the ocean.

However, in order to understand complex physical processes, it is often useful to apply simple models to build a background of information to be transferred to more elaborate configurations. In this view, this study analyzes the dynamics of the subtropical North Atlantic (NAtl) basin and the Gulf of Mexico (GOM), using a reduced-gravity model. There are two major purposes. The first is to verify the sensitivity of the solutions to the grid spacing. Instead of configuring the experiments over the same geographical domain with different grid resolutions, we have chosen to apply a coarse-resolution, basin-wide NAtl model and a fine-resolution GOM model. The use of the reduced gravity formulation drastically contained the computational cost, yet provided significant insight into the dominant dynamics. With this approach, we were also able to pursue the second goal: to couple the GOM regional model to the surrounding Caribbean Sea (CarSea) and verify the influence of the Yucatan Current (YucCur) variability on the Loop Current (LpCur) mesoscale activity.

In the following experiments, the NAtl model is forced by monthly climatological winds and by specification of the inflow transport from the South Atlantic Ocean; and the regional GOM model is forced by the climatological winds and by the inflow at the southern port as it is derived from the NAtl basin model.

Hurlburt and Thompson (1980) (henceforth referred to as HT) carried out the first extensive study of the LpCur using a wide range of model parameters and showed that periodic eddy shedding events can be obtained with steady flows prescribed at the Yucatan Strait (YucStr). Following models have mostly been configured on domains that partially include the CarSea and the NAtl basin off the eastern

Florida coast, to remove from the solutions those errors and inaccuracies which are caused by the specification of the open boundary at the Yucatan and Florida Straits (FlaStr). The models, usually forced by steady flows, are sensitive to the location of the YucCur (upstream the YucStr) and the distribution of the inflow transport along the southern opening (Dietrich and Lin, 1994) and suggest the importance of the CarSea dynamics as a forcing mechanism for the LpCur.

This paper is organized as follows: Section 2 describes the principal attributes of the numerical model. Section 3 discusses the results from the NAtl experiments and Section 4 from the GOM simulations. Finally, Section 5 is a concluding summary.

2. THE OCEAN CIRCULATION MODEL

The ocean circulation model is derived from the external mode equations for the solution of the vertically-integrated flow which are part of the 3-D free surface models that Prof. D. Haidvogel and his colleagues are developing at Rutgers University. The principal attributes of the Shallow Water Equation Model (SWEM) are:

- finite differencing
- Arakawa C-grid
- generalized boundary-fitted orthogonal coordinates
- option for masking out land areas.

The generalized orthogonal coordinates were introduced to avoid the numerical inaccuracies of approximating the coastlines by a step-like function (Arakawa and Lamb, 1977). In basin-wide applications, the complexity of the domain geometry makes it virtually impossible to adopt boundary-fitted grids. However, curvilinear coordinates give the opportunity to concentrate fine spatial resolution in areas of higher interest and minimize the number of masked land points, indeed, reducing the computational cost of using Cartesian coordinates over the whole domain at the required fine resolution.

Curvilinear coordinate systems may lead to abrupt changes of the grid cell size, and consequent numerical distortion of the traveling features. To contain this problem, the eddy viscosity coefficients are computed by an algorithm developed by J. Wilkins (Hedstrom, 1993). Unless otherwise specified, the lateral mixing co-

efficients in both Laplacian and biharmonic formulations are defined as a function of the Reynolds number, i.e., terms such as: $\nu 2(f_{\xi_1\xi_1} + f_{\xi_2\xi_2})$ are rewritten as:

$$\nu 2(\xi_1) f_{\xi_1\xi_2} + \nu 2(\xi_2) f_{\xi_2\xi_2} \quad \text{where} \quad \nu 2(\xi) = \nu 2_o \mathrm{d}\xi/\Delta\xi_o \tag{2.1a}$$

Similarly, the biharmonic viscosity coefficient, $\nu 4$, is written as follows:

$$\nu 4(\xi) = \nu 4_o (\mathrm{d}\xi/\Delta\xi_o)^3 \tag{2.1.b}$$

In eq. (2.1.) $\mathrm{d}\xi$ is the grid spacing and $\Delta\xi_o$ is a reference length scale. The parameters $\nu 2_o$ and $\nu 4_o$ are the reference Laplacian and biharmonic viscosity coefficient, respectively.

The model is configured in the reduced-gravity (or 1.5 level) formulation. That is, the model assumes a dynamically-active layer of fluid of thickness h and density ρ_1 lying over an infinitely-deep motionless layer of density ρ_2. The associated Rossby radius of deformation is:

$$L_R = \frac{\sqrt{\mathrm{g'h}}}{\mathrm{f}}, \quad \text{where} \quad \mathrm{g'} = \mathrm{g}\frac{(\rho_2 - \rho_1)}{\rho_o} \tag{2.2}$$

The surfacing of the layer interface has always been an issue for layer models. In the following simulations, the problem may arise in the North Atlantic subarctic gyre. To prevent outcropping of the upper layer, entrainment is locally activated when the upper layer thickness falls under 50 m. No net transfer of fluid across the interface is ensured by an equal detrainment applied over the rest of the basin.

2.1 The Boundary Conditions

Except at the in/outflow ports, the walls are rigid, and the no-slip condition is prescribed. At the inflow ports, the transports across and along the boundary are specified as external forcing fields. At the outflow ports the flow is computed in two steps:

- First, a modified Orlanski radiation condition is applied (Wallcraft, 1991), i.e.,

$$q_B'^{n+1} = \begin{cases} \frac{(1-\Lambda)q_B^{n-1} + 2\Lambda q_B^n}{(1+\Lambda)} & c > 0 \\ q_B^{n-1} & c \leq 0 \end{cases} \tag{2.3a}$$

where q is the across-boundary velocity and q' is an intermediate variable. The index B refers to the boundary points, (B-1) to the first interior points, and $\Lambda =$

$c(\Delta t)/(\Delta \xi)$. The local phase speed, c, is computed as in Camarlengo and O'Brien (1980):

$$c = -\frac{\Delta \xi}{\Delta t}\frac{q_{B-1}^{n} - q_{B-1}^{n-1}}{q_{B-1}^{n-1} - q_{B-2}^{n-1}} \tag{2.3b}$$

(positive sign is toward the boundary region).

The discrimination between the positive and negative values of the local phase speed is based on the different physics involved. When c is positive, the propagation of the interior solution is toward the boundary. When c is negative, information is carried away from the boundary, and the open boundary condition should be specified from a given external forcing.

- The second step ensures that the numerical scheme conserves the mass inside the basin, at least over a *long-term* period. Thus, the updated total transports across the outflow port, Q'^{n+1}, is nudged to the annual mean outflow value, Q_a. Finally, the velocity, q_B^{n+1} is computed as follows:

$$q_B^{n+1} = q_B'^{n+1} + 2\Delta t\, T_{ndg}\frac{(Q_a - Q'^{n+1})}{h_B^{n+1}\Delta \xi} \tag{2.3c}$$

where T_{ndg} is the nudging time scale.

3. THE NORTH ATLANTIC MODEL

Although the NAtl is perhaps the best observed of all the oceans, difficulties in producing a circulation scheme arise because data on the general dynamics and climatological fluctuations are still sparse and insufficient. However, there are 4 elements that are well supported by observations (Schmitz and McCartney, 1993)

1) The outflow transport at the FlaStr is about 30 Sv.
2) The net transformation of warm to cold water is about 13 Sv.
3) The rate of production of dense cold waters in the Nordic Seas is about 6 Sv.
4) The 30 Sv transported at the FlaStr increases roughly to 100 Sv south of Nova Scotia, due to instability of the main stream and recirculation of the wind-driven gyre.

To combine these 4 elements is one of the major challenges for producing a description of the NAtl large-scale dynamics. Several studies attempt to solve the

problem. Among them, Roemmich and Wunsch, (1985), suggest that the Sverdrup interior balance along 24N needs to account for 17 Sv of wind-driven outflow from the FlaStr which is joined by a larger transport (about 25-30 Sv) of the returning flow north of the Bahama Rise. This pattern clearly conflicts with other transport estimates at the FlaStr. Schmitz and McCartney (1985) describe a NAtl circulation which includes an upper-layer thermohaline contribution of 13 Sv from the South Atlantic Ocean (SAtl) x that compensates a net lower-layer southward cross-equatorial flow. The SAtl inflow moves inside the CarSea, passes through the FlaStr, transits the Gulf Stream system, and exits through the North Atlantic Current after recirculation and modification.

Ocean models also provide insight to the understanding of the NAtl circulation. Thompson et al. (1993) prove that the inclusion of the SAtl inflow drastically increases the accuracy of the solution in the Gulf Stream region and provides more realistic estimates of the mean flow transport and eddy kinetic energy field at middle latitudes.

Within the limits of the model configuration (viz., grid resolution), the large-scale features of the NAtl dynamics are analyzed in the following sections.

3.1 The Model Configuration

The numerical domain of the NAtl simulations takes full advantage of the flexibility of the curvilinear transformation. The numerical domain for the NAtl is illustrated in Fig. 3.1, and the model parameters are summarized in Table 3.1. In spite of the limited number of mesh points, the grid concentrates a fine spatial resolution in the GOM, CarSea, and along the U.S. East Coast. An important geographical feature, also represented by the grid, is the Windward Passage (WinPas), the opening between Cuba and Hispaniola Islands. Maps of the NAtl and place names used in the text are illustrated in Fig. 3.2.

All the experiments described in this document are first conducted in a closed domain. Tests with open boundary conditions specify the northern boundary between Iceland and Norway as an outflow port and the transect between South America and western Africa as an inflow port. The inflow condition is given as a uniform current, about 100 km wide, that flows along the South American coast, whose transport value ensures an outflow of about 30 Sv at the FlaStr.

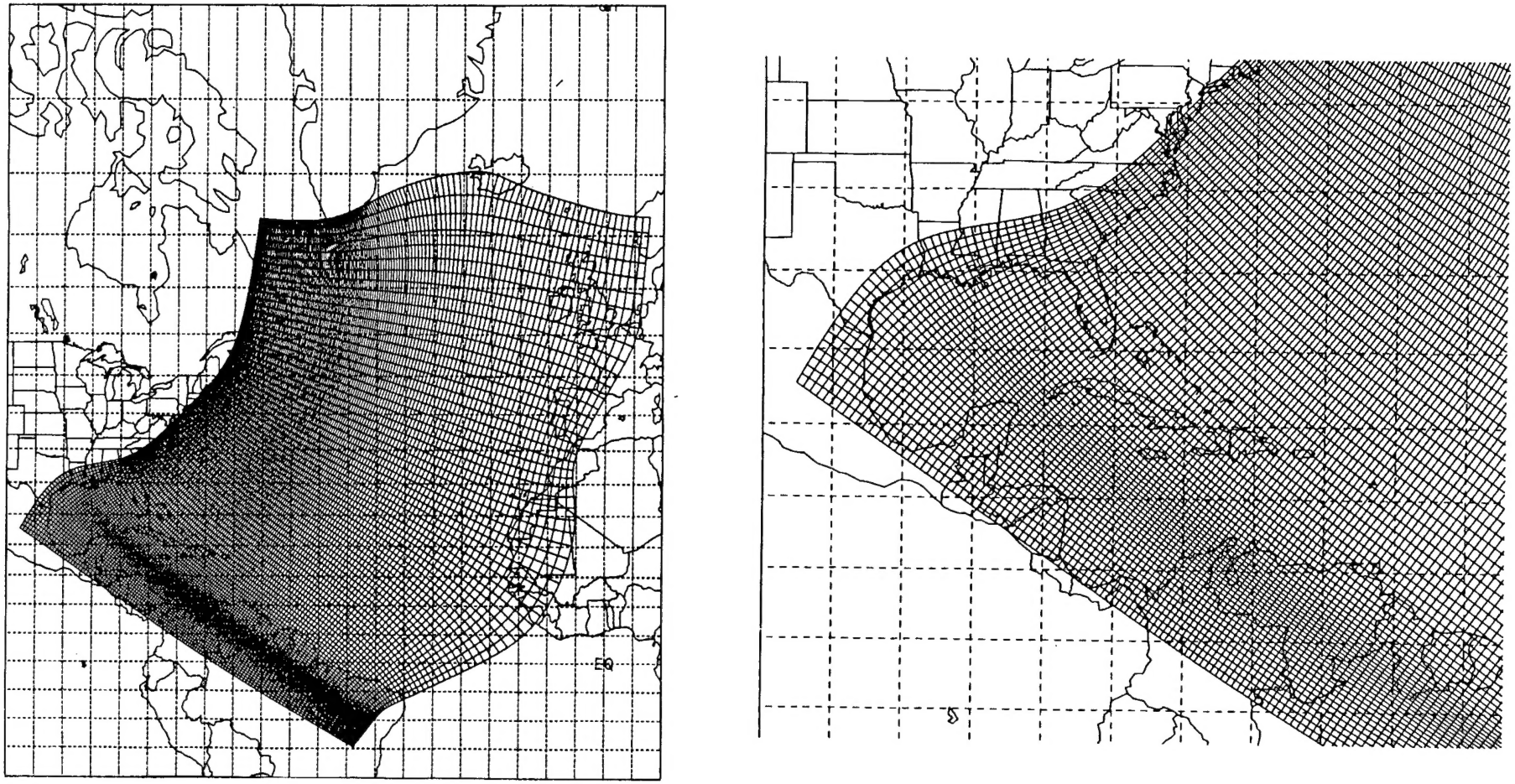

Fig. 3.1: The North Atlantic Ocean numerical grid and the enlarged portion of the Caribbean Sea and Gulf of Mexico.

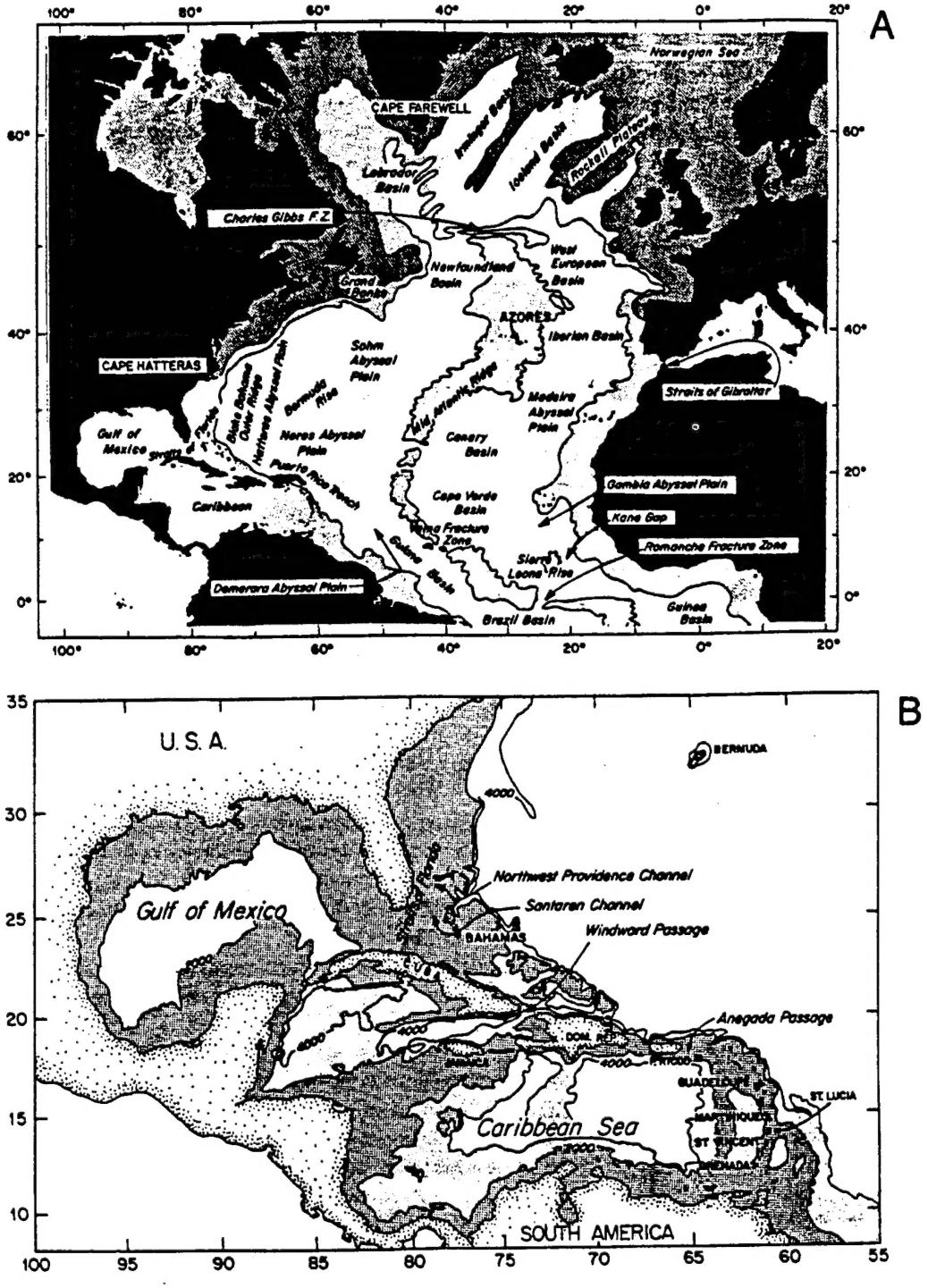

Fig. 3.2 : Maps and place names of the NAtl basin. From Schmitz and McCartney (1993).

The model is forced by the climatological monthly wind stresses from Hellerman-Rosenstein (1983) which are linearly interpolated over time every day (Peggion and Foo, 1994). In order to remove from the solution those features generated by a forcing impulsively applied to an initially resting ocean, the wind stress magnitude and the inflow transport are linearly ramped from zero to the prescribed value over one year. This initial period is never counted, and the simulations are restarted at t=0. Unless otherwise specified, all the results are relative to the tenth year of simulations.

Table 3.1a The NAtl Model Parameter

total grid points	L*M	129x97
geographical extension	xl*el	12,600 x 11,310 (km)
latitude range		15S - 65N
longitude range		100W - 5E
eddy viscosity coefficient	$\nu 2_o$	100 $m^2 s^{-1}$
viscosity spatial reference	$\Delta\xi_o$	25 km
outflow nudging time scale	T_{ndg}	1 day^{-1}
reduced-gravity accel.	g'	0.02 ms^2
bottom drag coefficient	C_D	2.6e-6 ms^{-1}
density reference	ρ_o	1000 kgm^{-3}

Table 3.1b The Spatial Grid Resolution of the NAtl Domain.

	min	max	NA	GOM	CarSea
$\Delta\xi_1$ (km)	11	231	51	35	43
$\Delta\xi_2$ (km)	20	236	79	37	22

The range of the spatial resolution and the average values over some geographical regions of the NAtl model geometry. ξ_1 and ξ_2 are the coordinates associated with the top and right boundary, respectively.

3.2 The Numerical Experiments

Although the grid is far from being suitable for a realistic eddy-resolving solution, it is possible to define the initial thickness of the upper layer, such that features on the order of the Rossby radius of deformation are solved at least in the areas of fine spatial resolution, and to verify the sensitivity of the model to the grid spacing. The numerical simulations are, henceforth, divided into two broad groups: the eddy-resolving (h= 1250 m, L_R =50 km) and no-eddy-resolving experiments (h= 450 m, L_R =30 km). Table 3.2 summarizes the attributes of the numerical experiments.

Table 3.2 The NAtl Numerical Experiments

Experim	h (m)	L_R (km)	SAtl infl
NAtl_1	1250	50	closed
NAtl_2	1250	50	11 Sv
NAtl_3	450	30	closed
NAtl_4	450	30	17 Sv

Fig. 3.3 shows the annual mean distribution of the upper layer thickness anomaly. The structure of the subarctic gyre is unrealistic due to the northern boundary configuration. With closed boundary conditions, there is a strong inward current at the Greenland eastern coast that recirculates south of the Denmark Strait. This feature is removed when the southern tip of Greenland is not included in the basin model geometry. In that case, the gyre presents a strong western intensification at the northwestern corner.

The western intensification of the subtropical gyre is well reproduced. In all the simulations, the center of the gyre is located somewhere south of Cape Hatteras. In the proximity of Cape Hatteras, the Western Boundary Current splits into two branches. One branch separates from the coast, moves into the central part of the basin, and joins the return flow of the subtropical gyre. The other branch flows northward, separates at Newfoundland, and feeds the jet that divides the

SEA SURFACE DISPLACEMENT

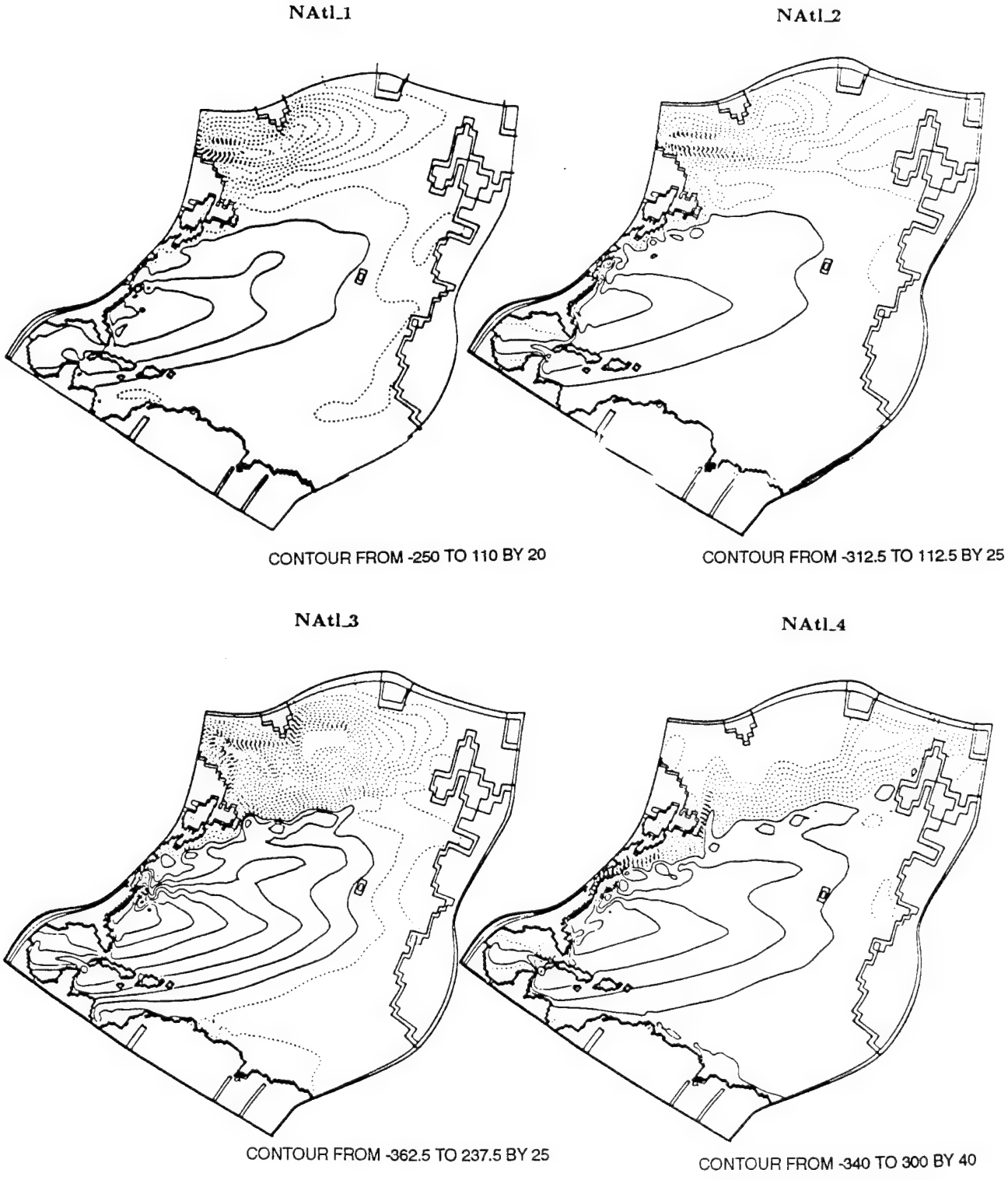

Fig. 3.3 : The annual mean of the sea surface displacement.

double gyre system. The current moves toward Northern Ireland, and its location is consistent with other NAtl circulation models (Thompson et al., 1993).

All the experiments produce mesoscale activity in the proximity of Cape Hatteras, with large excursions of the current axis and eddy shedding events. With the specification of the SAtl inflow the variability becomes more energetic, the separation point moves northward with a large meander that encloses a strong warm-core ring. The ring may detach from the main stream, but it is rapidly reabsorbed. After the separation from the coast, the axis of the main current moves further into the inner basin and experiences large meanders and fluctuations.

The subarctic gyre and the location of the jet that separates the gyres are not significantly affected by the wind seasonal variability, as twin experiments forced by the annual mean wind have shown. The subtropical gyre is much more affected by the wind variability. Many aspects of the seasonal fluctuations of the basin-wide circulation depend upon Rossby waves which are the principal means by which the ocean adjusts to the variations of the atmospheric forcing. The presence of Rossby waves is indicated by the Empirical Orthogonal Function (EOF) decomposition applied to the daily records of the upper layer thickness. The first EOF modes are depicted in Fig. 3.4, and the amplitudes of the first 4 modes are illustrated in Fig. 3.5. Table 3.3 summarizes the dominant frequencies of the EOF mode time series.

Table 3.3 The Dominant Frequencies of the EOF Modes From the NAtl Simulations

Experim.	Mode 1	Mode 2	Mode 3	Mode 4
NAtl_1	360	360	360-195	195-90
NAtl_2	360	360	360-90	90-360
NAtl_3	360	360	360-200	360-180
NAtl_4	270	245	225	225

The dominant periods (in days) of the first EOF modes of the numerical experiments. Second values refer to the secondary significant peaks of the time series frequencies.

EOF MODE # 1

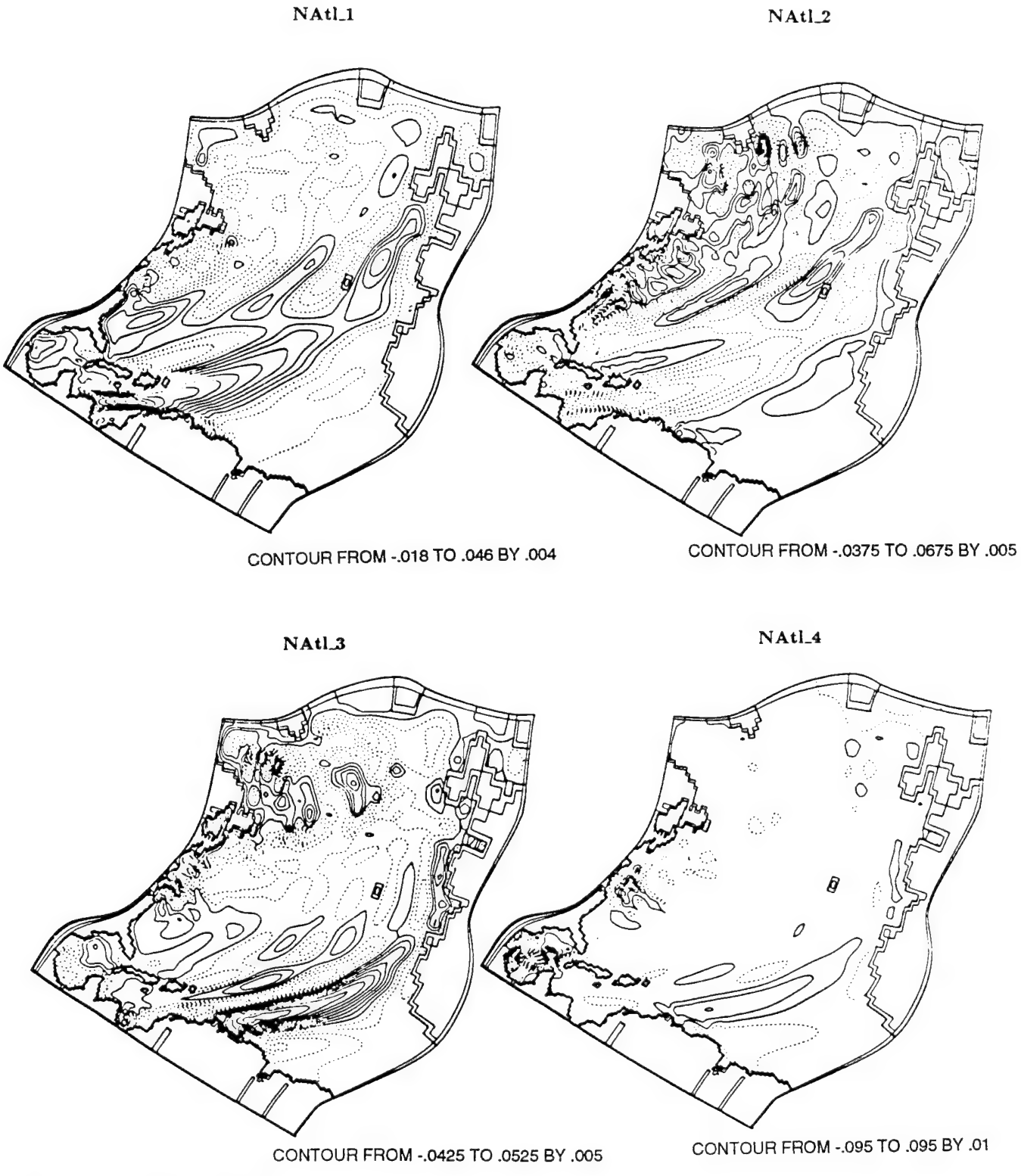

Fig. 3.4 : The EOF First mode.

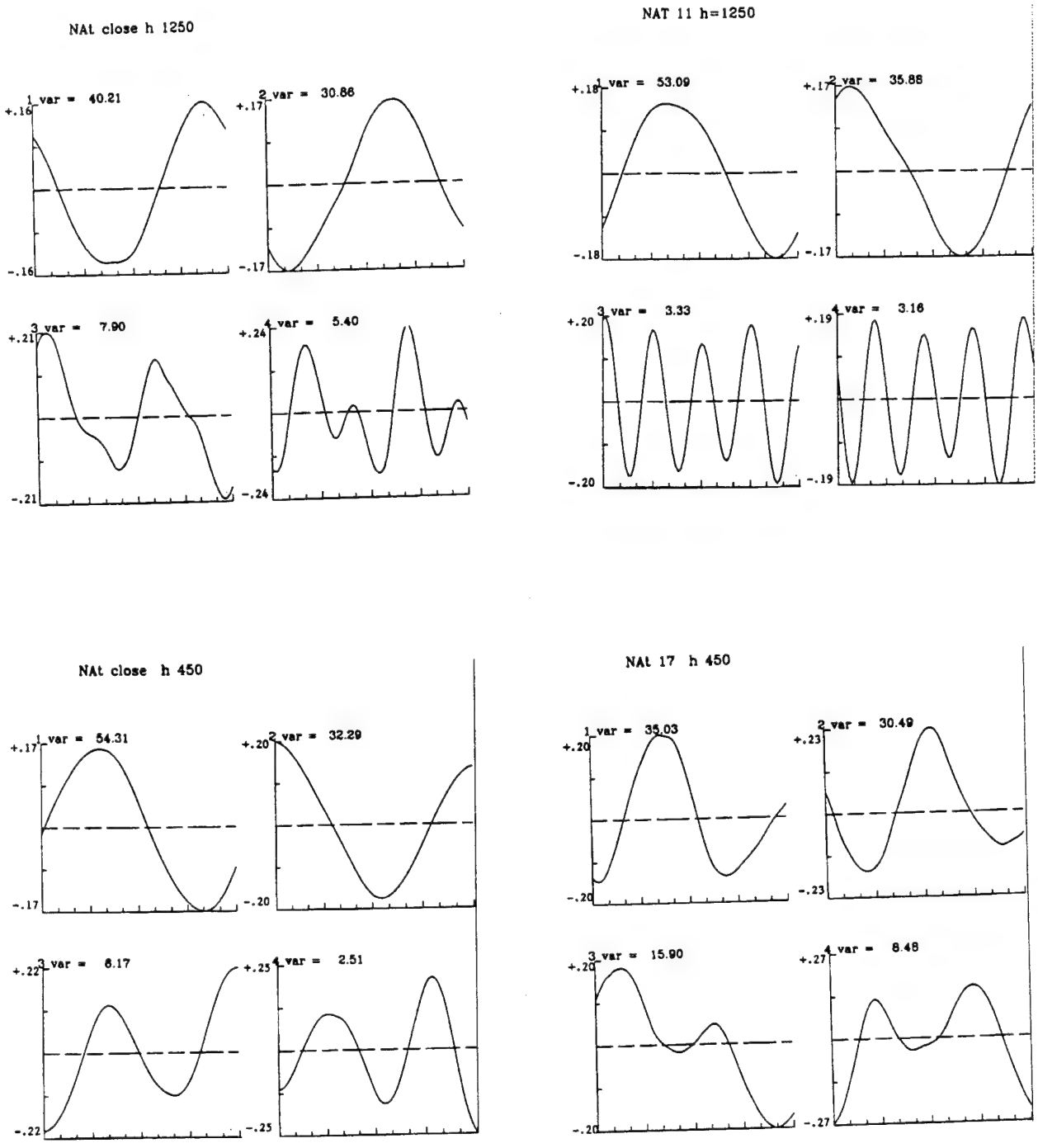

Fig. 3.5 : The deviation from the mean value of the EOF mode amplitude from the NAtl experiments over a one-year cycle.

The first EOF mode indicates that the eastern basin is dominated by the Rossby waves traveling across the domain, at an approximate angle of 30 ^{o} with the parallels; the western basin is dominated by the mesoscale variability of the subtropical gyre. Indeed, the same pattern is also present in the solution of NAtl_4, where the increased mesoscale variability inside the GOM partially removes the Rossby wave signal. In the other simulations, the GOM variability is not apparent before the 3rd mode (i.e., the GOM circulation contributes very little to the overall fluctuation of the NAtl basin).

3.2.1 The western tropical basin

The geometry of the western, tropical NAtl has a strong effect on the large-scale circulation and Rossby wave propagation. The simulations indicate that part of the return flow of the wind-driven gyre enters the CarSea in correspondence with the Windward Islands, and some flows into the WinPas. Both branches move inside the GOM and return to the subtropical gyre from the FlaStr. There is a third component that moves outside the CarSea along the northern boundary of the Greater Antilles Islands, joins the flow from the FlaStr, and feeds the Florida Current.

The circulation inside the CarSea is characterized by the Rossby waves impinging the Central American coast. Rossby waves enter the CarSea at approximately a 60^o angle with the coast, creating a shadow zone in the southern part of the Colombian basin. As the waves impinge the Nicaraguan coast, part of their energy is reflected southward along the Central and South American coast, exits the CarSea, and recirculates backward inside the inner NAtl basin.

The absence of the Windward Islands in the numerical grid configuration has a deep effect on the CarSea circulation. Not inhibited by the real topographic features, most of the reflected Rossy waves can leave the CarSea. In other high-resolution NAtl models the passages between the Windward Islands allow the incident waves to enter the CarSea, but only a smaller portion of the reflected waves can leak outside (Townsend, personal communication). Due to this unrealistic configuration of the western tropical basin, the model requires a higher (than the usually accepted) value for the SAtl inflow to match the observed transport at the FlaStr.

Windward Passage

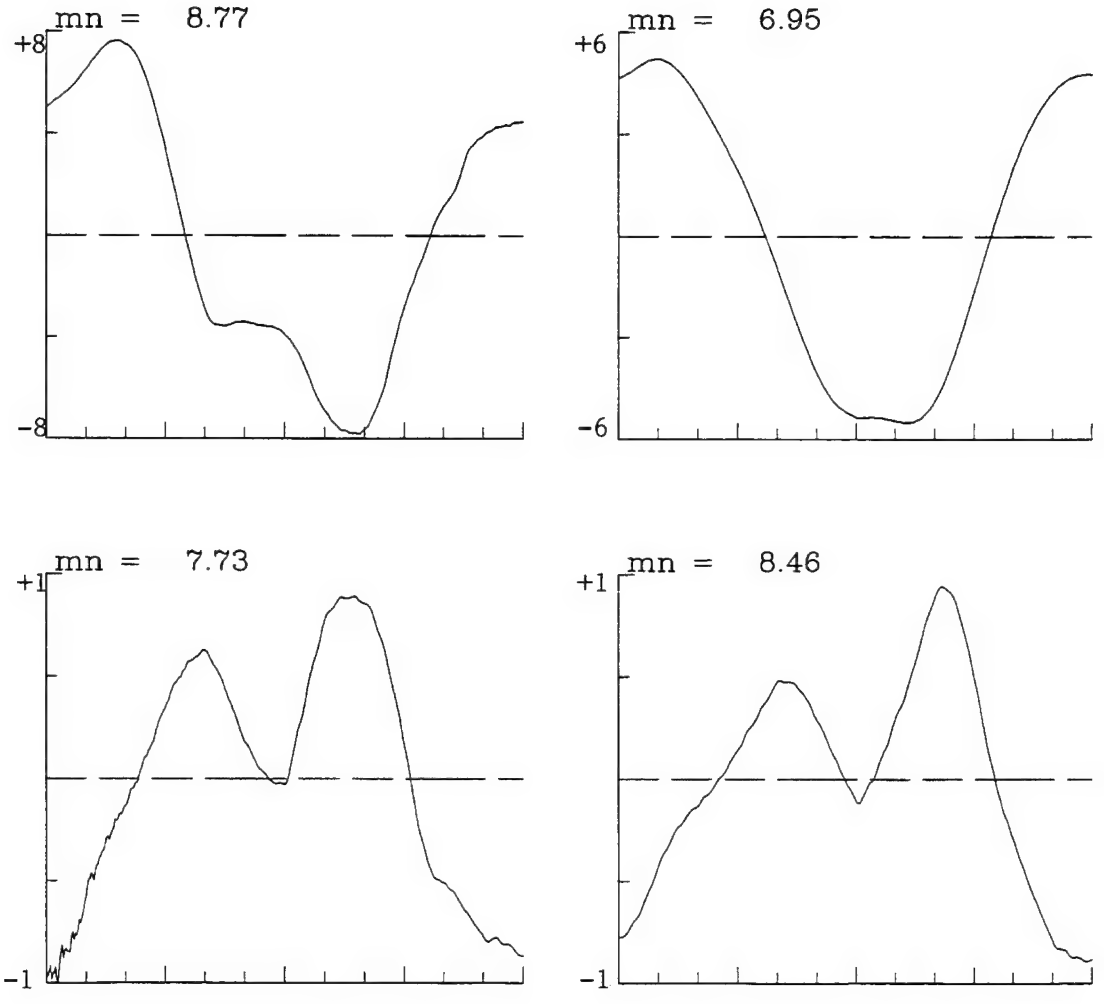

Fig. 3.6 : The deviation from the mean value of the transport at the WinPas over a one year cycle.

The role of the narrow passages that connect the CarSea and the central NAtl basin, is outlined by the circulation through the WinPas. Fig. 3.6 illustrates the time series of the inflow transport (toward the CarSea) as computed by the numerical experiments. The transport variability through the WinPas is highly dependent upon the specification of the Rossby radius. In the experiments NAtl_1 and NAtl_2 the flow fluctuations are dominated by the Rossby waves (Fig. 3.4); in NAtl_3 and NAtl_4 the flow is more uniformly distributed over time. All the simulations indicate an annual mean transport of about 7 Sv that is in agreement with the estimates of Roemmich (1981).

The two components that enter the CarSea from the WinPas and the broad southern opening organize in a narrow western current north of the Nicaraguan coast. The current supports barotropic and baroclinic instabilities. All the experiments indicate the presence of small eddies (length scale of about 50 km) that are generated south of the YucStr and sometimes propagate inside the GOM carried by the main stream. In NAtl_4 this mesoscale variability is highly energetic with oscillations of the eastern edge of the YucCur and eddy shedding. Fig. 3.7 is a snapshot at Day 82 of the western tropical NAtl from the NAtl_4 simulations. Maul (1977) suggests that when the eastern edge of the YucCur is at the Mexican coast, part of the flow may recirculate southward and be reabsorbed by the main stream. Small eddies (about 10-15 km in diameter) imbedded in the main current at the YucStr have been observed, and they may be as well related to the fine structure of the LpCur in the mid-Gulf (Maul et al., 1974).

Table 3.4 Transport Values

Exper	Car Sea		WndPas	YucStr	RetFl	FlaCur
NAtl_1	10.85	(6.73)	8.77	19.62	23.88	43 .50
NAtl_2	21.87	(4.73)	6.95	28.82	23.82	52 .64
NAtl_3	7.15	(4.98)	7.73	14.88	27.67	42 .25
NAtl_4	22.65	(5.52)	8.46	31.11	25.44	56 .55

The net transport values (in Sv) in the western tropical NAtl. See Sect. 3.2.1 for definition of terms.

Table 3.4 summarizes the net transports as computed by the numerical experiments. The CarSea values in parentheses refer to the recirculating transports out of the sub-basin. The return flow is defined as the difference between the FlaCur transport (computed approximately at 24N) and the FlaStr outflow.

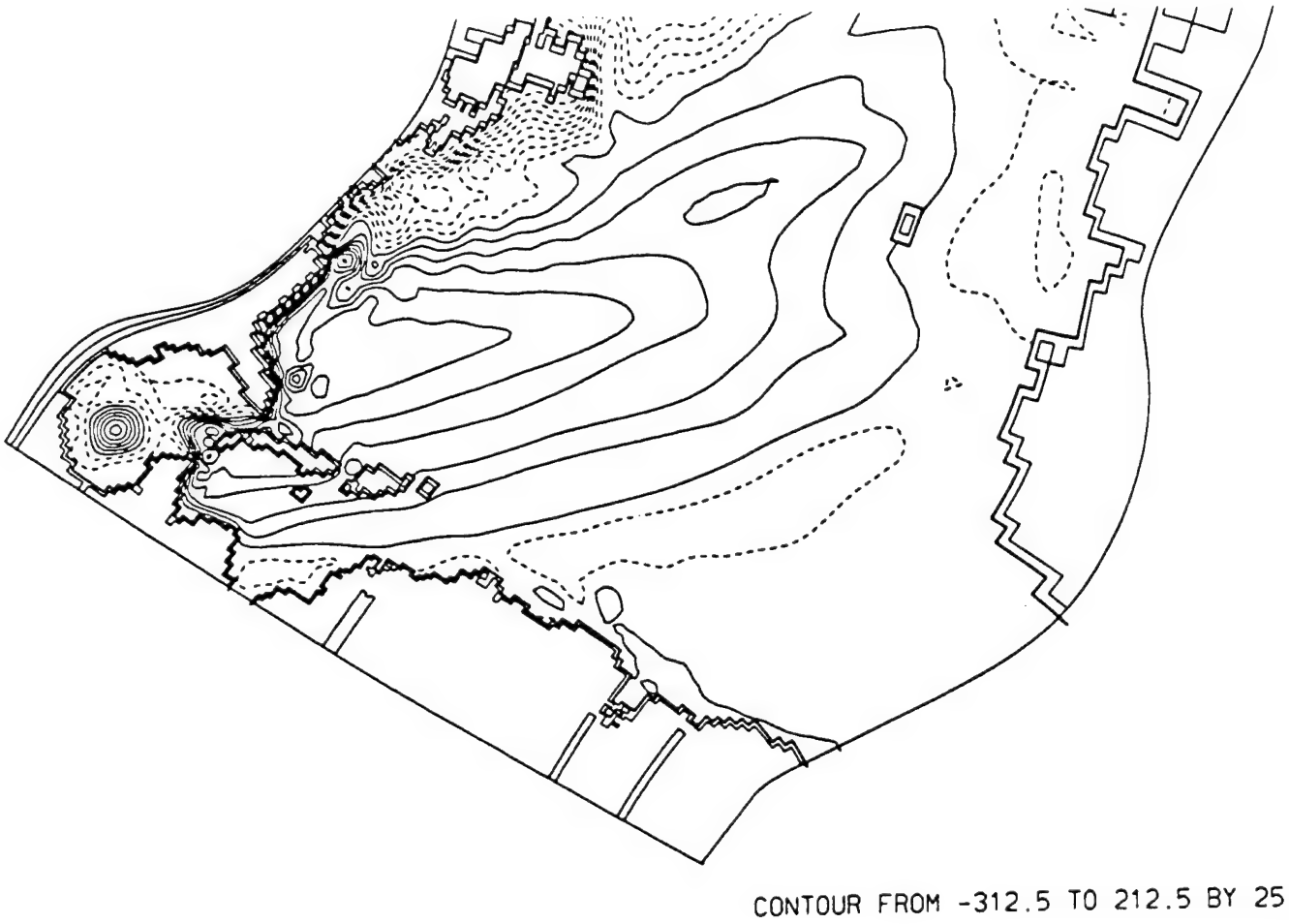

Fig. 3.7 : Snapshot of the sea surface displacement of the western subtropical NAtl from experiment NAtl_4.

3.2.2 The GOM circulation from the NAtl experiments

The annual cycles of the Yucatan inflow are illustrated in Fig. 3.8. It is found that the time series of NAtl_1−3 are quite asymmetric, with a broad maximum in July/August, followed by a sharp drop to the minimum values of September. In NAtl_4, the inflow transport is less affected by the seasonal wind variability (i.e., the prescribed SAtl inflow dominates the YucCur), and the fluctuations of the record are mostly associated with the mesoscale variability of the YucCur, as discussed in the previous section.

In spite of the simplicity of the dynamics represented by the 1.5 level formulation, the numerical experiments reproduce the general pattern of the GOM circulation, although the spatial and temporal scales of the LpCur fluctuations are not always realistic. The LpCur is highly dependent upon the specification of the Rossby radius. The experiments NAtl_1 and NAtl_2 generate eddy shedding events at approximately 3 month intervals; and the main stream is generally tilted westward, with the left edge often at the northern shore of the Yucatan Peninsula. It might be possible that the incorrect orientation of the LpCur be a consequence of the local winds. Reid (personal communication) suggests that climatological, global wind data sets may not be suitable for modeling the GOM, because they do not take into account the orographic effects from the high mountain chain along the Mexican coast. Experiments NAtl_3 and NAtl_4 present a more realistic eddy shedding at a rate of about 6-7 months; excursions of the LpCur are also more toward the central part of the basin.

Additional tests indicate that the time scale of the LpCur oscillations are not affected by the specification of the eddy viscosity coefficients. At high viscosity values, the LpCur may not shed and instead form large meanders (that eventually reach the western coast), yet at the same frequency. At lower viscosity, there is no penetration of the LpCur. Eddy shedding occurs just off the western side of the YucStr, and rings move westward fast. The limit cases have no detached rings and no penetrations of the LpCur which flows directly along the Cuban coastline and exits the basin. The size of the rings is proportional to the eddy viscosity coefficients and may range from 100 to 250 km in diameter.

If a detached eddy or meander reaches the western shelf, a smaller (half or less in size) cyclonic ring forms north of the impinging feature, moves far away, and

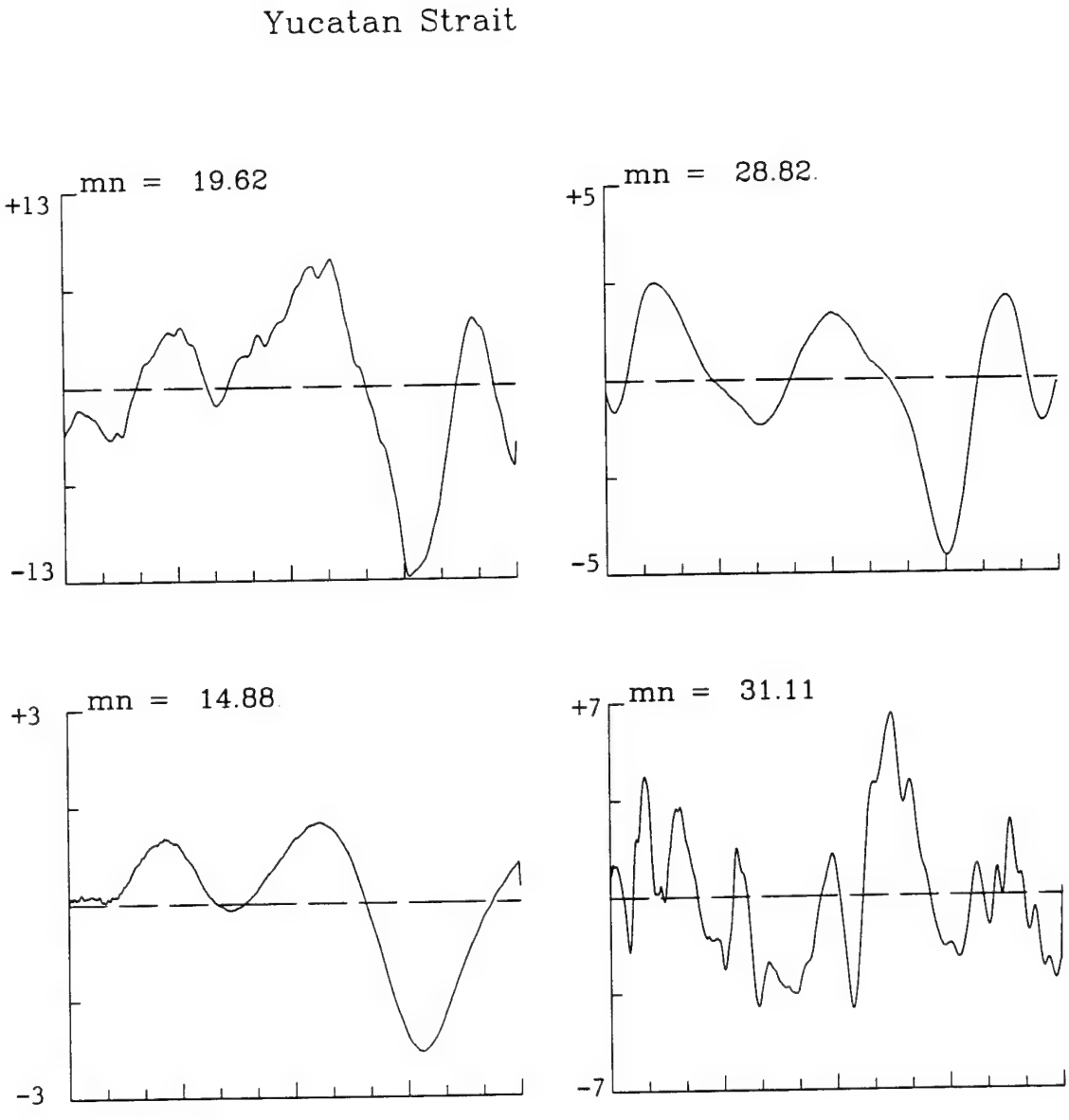

Fig. 3.8 : The annual transport at the YucStr. Same as Fig. 3.6.

is dissipated. The genesis of the paired eddies has been extensively observed (Brooks and Kelly, 1986, Vidal et al., 1992). It has been speculated and numerically verified (Dietrich, 1993) that the downwelling ahead of the warm-core ring is compensated by an upwelling associated with the Ekman boundary layer over the continental slope and shelf break region. However, the 1.5 level formulation cannot parameterize the vertical distribution of water masses, and/or the interactions with topography. Thus, the paired eddy formation appears more in line with the *violent collision* mechanism described by Shi and Nof (1993). The authors demonstrate that when a warm core eddy collides with a lateral wall, there is a leak of fluids that forms a smaller (1/3 in size) cyclonic ring to the right of the boundary. Due to mutual advection, the eddies move further away from each other.

The time series of the transport out of the FlaStr are plotted in Fig. 3.9. All the experiments provide a minimum value during the September/October months, which are related to local winds (Schott et al., 1988). The correlation factors between the Florida transport and the winds (computed in the proximity of the Martinica Island) are high (.70 and more), with a phase shift of about 20 days.

An attempt has been made also to evaluate the correlation between the Yucatan and Florida transports. It follows that the inflow and outflow transports are not strongly correlated. Although both records generally show the strong minimum value during September, the correlation is lost because of the quite different variance distributions of the time series. The Yucatan inflow has greater variation than the Florida transport, which is more steady and uniformly distributed over time. At high viscosity values, the correlation improves, but so does the correlation between the winds and the Yucatan transport. This is not surprising; high lateral mixing inhibits the genesis of barotropic and/or baroclinic instabilities of the YucCur, and the wind forcing becomes the most dominant dynamical mechanism.

Fig 3.10 shows the differences between the inflow and outflows, which are representative of the variations of the water mass inside the GOM. Maul (1977) observes that an excess of inflow over the FlaCur is required to make the LpCur grow and prepare the conditions for eddy shedding. The events reported in Table 3.5 are usually corresponding to variations of the Yucatan transport, but not all the maxima of the variance distribution are associated with eddy shedding or significant meander formations of the LpCur.

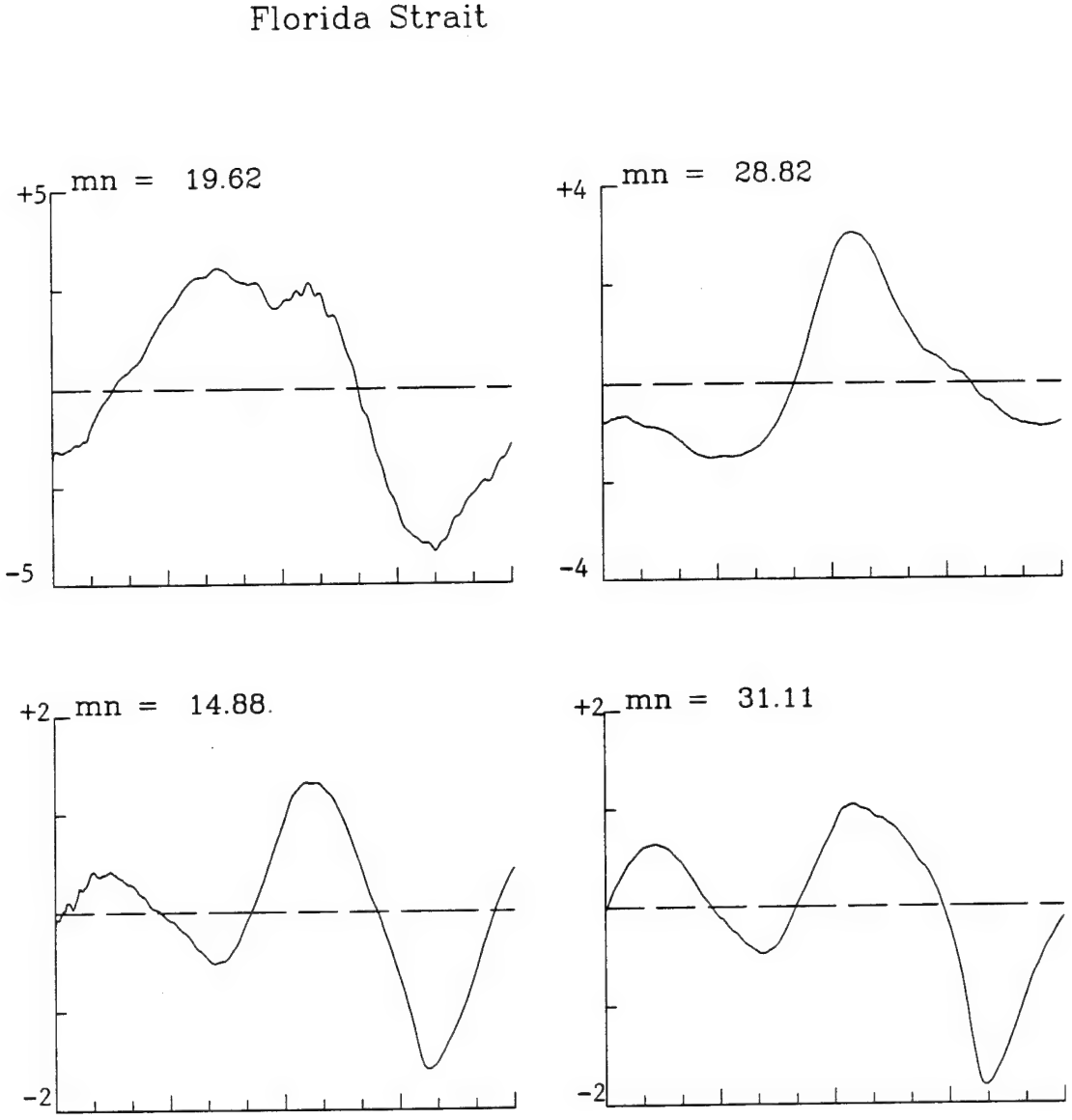

Fig. 3.9 : The annual transport at the FlaStr. Same as Fig. 3.6.

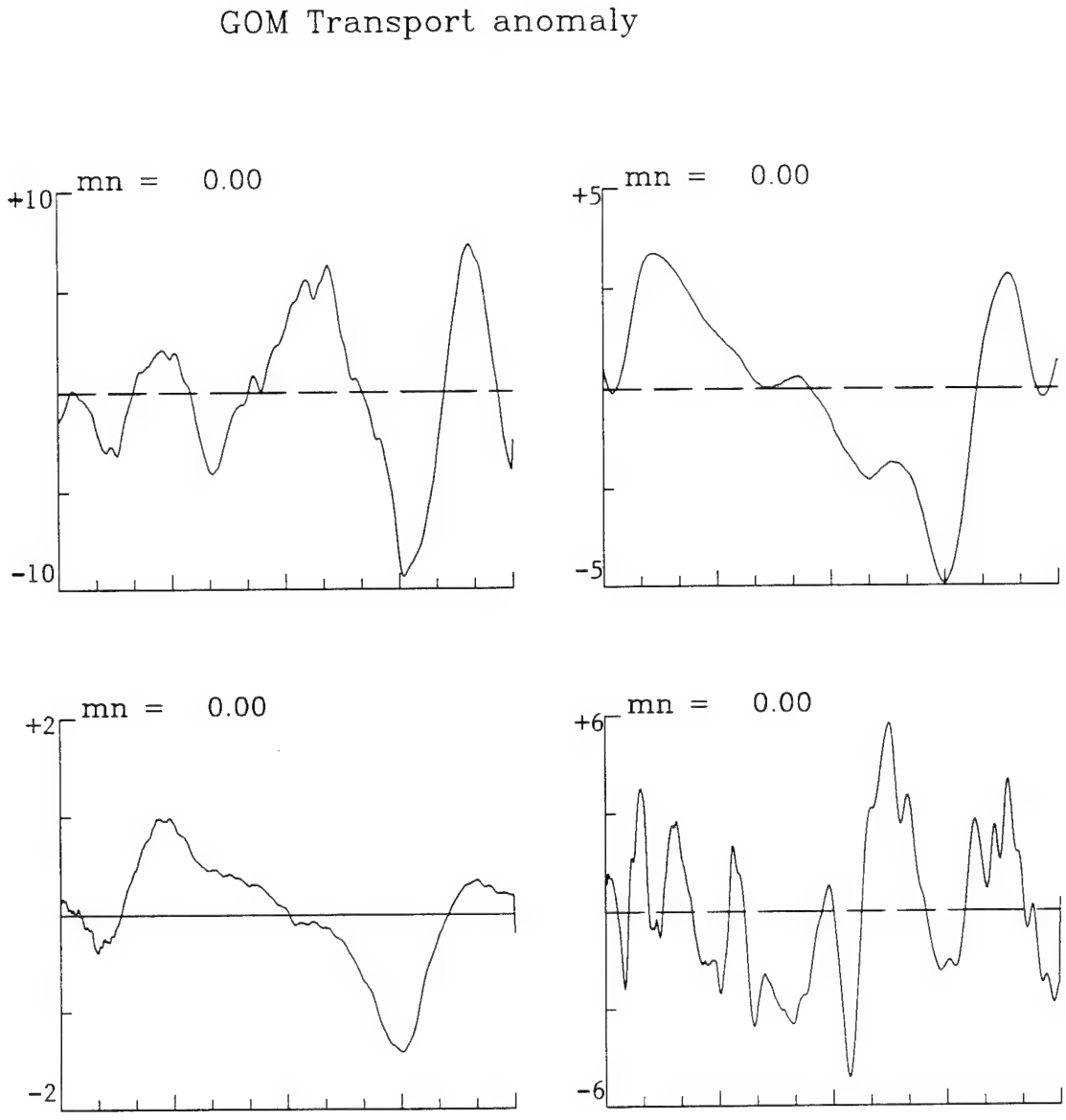

Fig. 3.10 : The GOM annual transport anomaly. Same as Fig. 3.6.

Table 3.5 The LpCur Variability

Experim.	NAtl	GOM
1	4 eddies	4 eddies
2	2 eddies +1 meand.	3 eddies
3	2 eddies	2 eddies
4	1.5 eddy	1.5 eddy

The LpCur annual events from the NAtl and GOM numerical simulations.

4. THE GULF OF MEXICO MODEL

The Loop Current is the dominant feature of the GOM circulation. It enters through the YucStr, moves northward, loops and exits the FlaStr. Observations indicate that when the LpCur has penetrated north of 24N, an instability may develop and an anticyclonic ring may detach from the main stream. If the ring is not reabsorbed, it propagates westward. As it approaches the western shelf, it dissipates; and a smaller cyclonic eddy often forms to the north (Cooper et al., 1990). The rings typically have diameters of about 360 km, a depth signal of about 1000 m, and a mean translation speed of about 2.1 km/day. Approximately 1-3 rings may separate each year (Elliott, 1979).

Several numerical models have investigated the dynamics of the GOM. HT first studied the LpCur instabilities using a two-layer and a reduced-gravity model. They show that the time variations of the YucStr transport are not essential for eddy shedding, but rather the process depends upon the horizontal shear instability of the first internal mode. This work was completed by Wallcraft (1986) suggesting that by the time the LpCur is configured for a new eddy shedding event, the previous ring has moved far away and has partially dissipated. This is in contrast with drifter observations (Lewis and Kirwan, 1987) which indicate that new rotational features of the LpCur may develop even before the previous ring is fully pinched off and which support an estimate of an average of 3 ring formations per year.

Blumberg and Mellor (1985), and Oey (1995), using a 3-D σ-coordinate model, simulate the basic features of the GOM dynamics and verify the sensitivity of the solution to the grid resolution and mixing coefficients. Dietrich and Lin (1994), using a 3-D rigid lid model, indicate the importance of the topographic β-effect and higher- order baroclinic modes in dissipating the rings as they approach the western shelf.

4.1 The Model Configuration

The grid domain of the GOM simulations is illustrated in Fig. 4.1, and the model parameters are summarized in Table 4.1. The model is forced by the monthly climatological winds and by the inflow transport at the right boundary. (Since the GOM domain overlaps with the NAtl grid, the dimensionless coordinates ξ_1 and ξ_2 are significantly rotated with respect to the longitude and latitude.

Table 4.1 The GOM Model Parameters

total grid points	L*M	129x97
geographical extension	xl*el	2,440 x 2,257 (km)
minimum grid resolution	$\Delta\xi_{\min}$	5.1 km
maximum grid resolution	$\Delta\xi_{\max}$	31.4 km
eddy viscosity coefficient	$\nu 2_o$	50 $m^2 s^{-1}$
viscosity spatial reference	$\Delta\xi_o$	25 km
outflow nudging time scale	rndg	6 hrs^{-1}

The model parameters for the GOM simulations. See Table 3.1 for unreported variables.

The inflow distribution is computed by interpolating the NAtl solution at the GOM port, daily over a one-year cycle. At the FlaStr, the outflow OBC described in Sect. 2.1 have been applied.

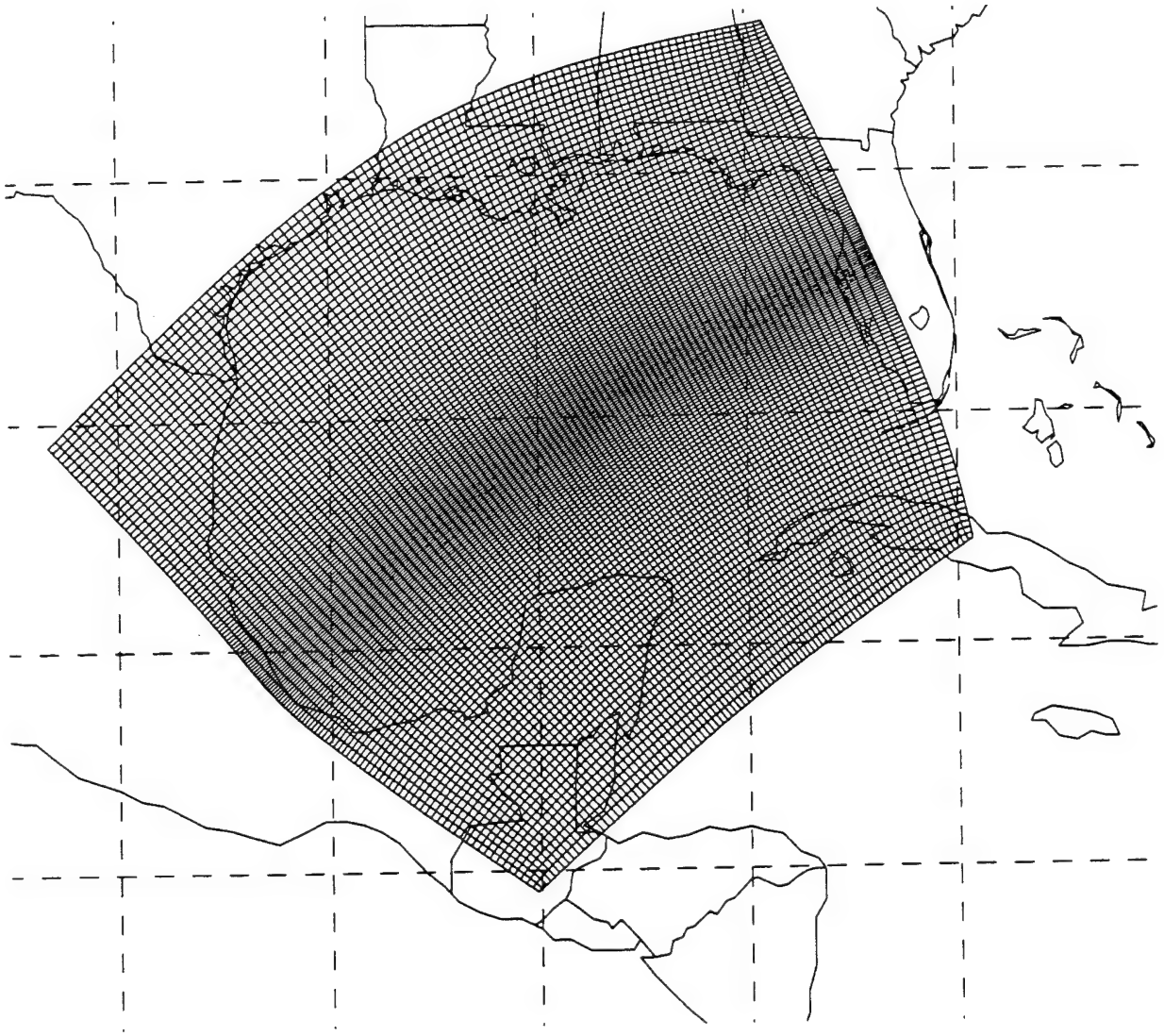

Fig. 4.1 : The numerical grid of the GOM regional model.

4.2 The Numerical Experiments

Fig. 4.2 illustrates eddy shedding events, and Table 4.2 summarizes the main characteristics of the anticyclonic features. As Table 3.5 also indicates, the time scale of the LpCur variability is not dependent upon the different grid resolution of the NAtl and GOM domains. Similarly, no significant differences were found in the values of Table 4.2 as compared with the NAtl solutions.

Table 4.2 The Main Features of the GOM Anticyclonic Rings

Experim.	Radius	SSA	Migrat.	Rotat
GOM_1	185	114	7.8	89 (15.1)
GOM_2	175	171	7.3	84 (15.1)
GOM_3	205	240	4.3	74 (20.1)
GOM_4	240	440	4.7	78 (22.3)

The averaged radius (km), upper layer maximum anomaly (m), westward migration velocity (km/day), and maximum rotation velocity (cm/s) of the LpCur detached rings. Values in parentheses are the period (in days) to complete a full rotation.

It follows that in experiments GOM_1–3 the cycles of the eddy separation are quite similar. The *unperturbated* path of the LpCur does not penetrate much inside the basin, and it is mostly located in the southern boundary and along the Cuban coast. Eddies are usually pinched off as soon as the internal swirl of the LpCur is fully developed and interact little with the main stream. After the swirl inside the LpCur is formed in GOM_4, the eddy interacts with the main stream before being completely separated. As Fig. 4.2d indicates, the eddy first separates at about Day 270, it is reabsorbed, and the real shedding occurs around Day 310.

As the eddies are pinched off, they migrate westward at the mean velocity values of Table 4.2. HT indicates that the westward migration of the anticyclonic rings depends upon the phase speed of the internal nondispersive and dispersive Rossby

GOM_1

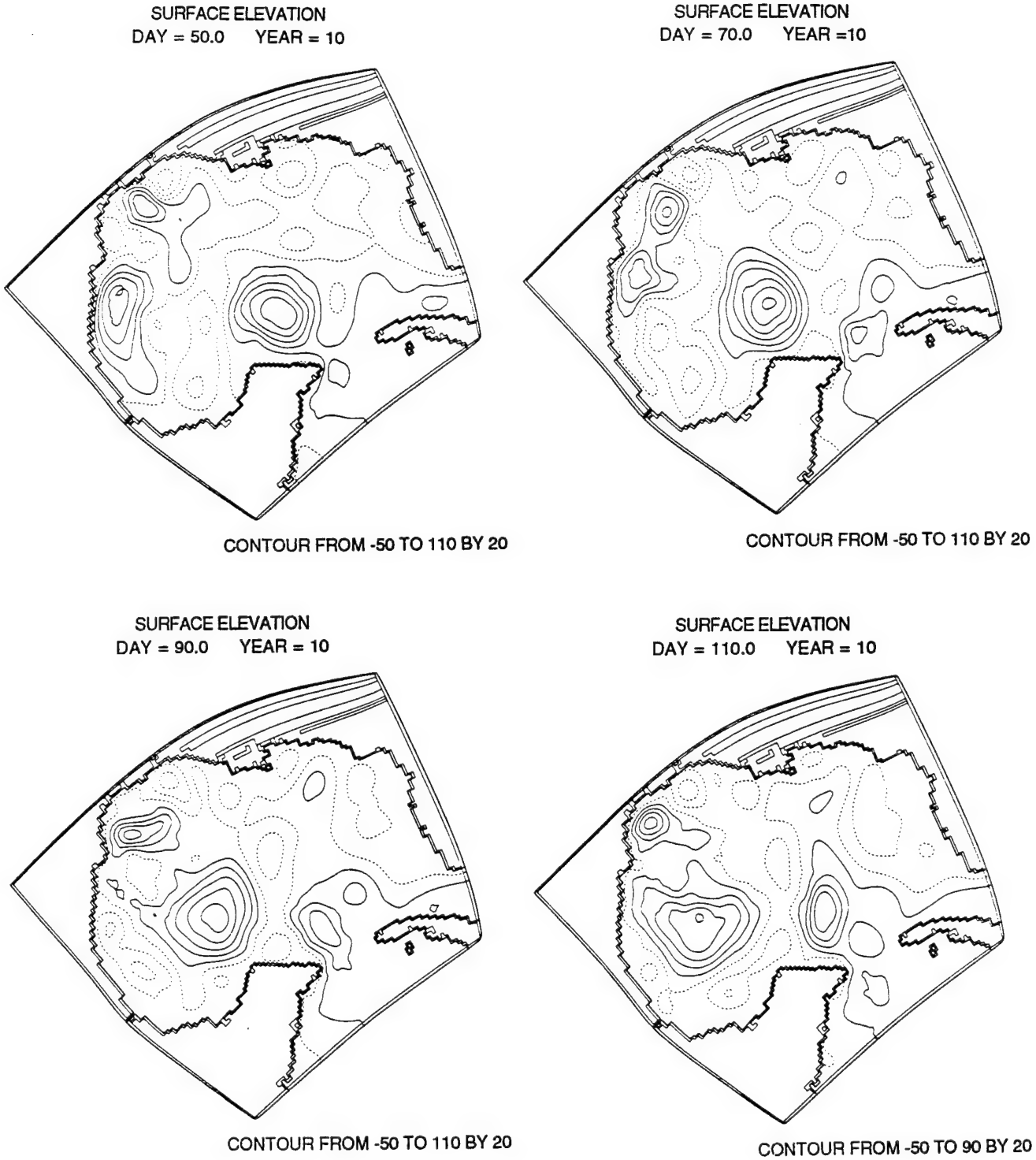

Fig. 4.2a : An eddy shedding event from GOM_1. Time interval: dt= 20 d, contour interval: $d\eta$=20 m.

GOM_2

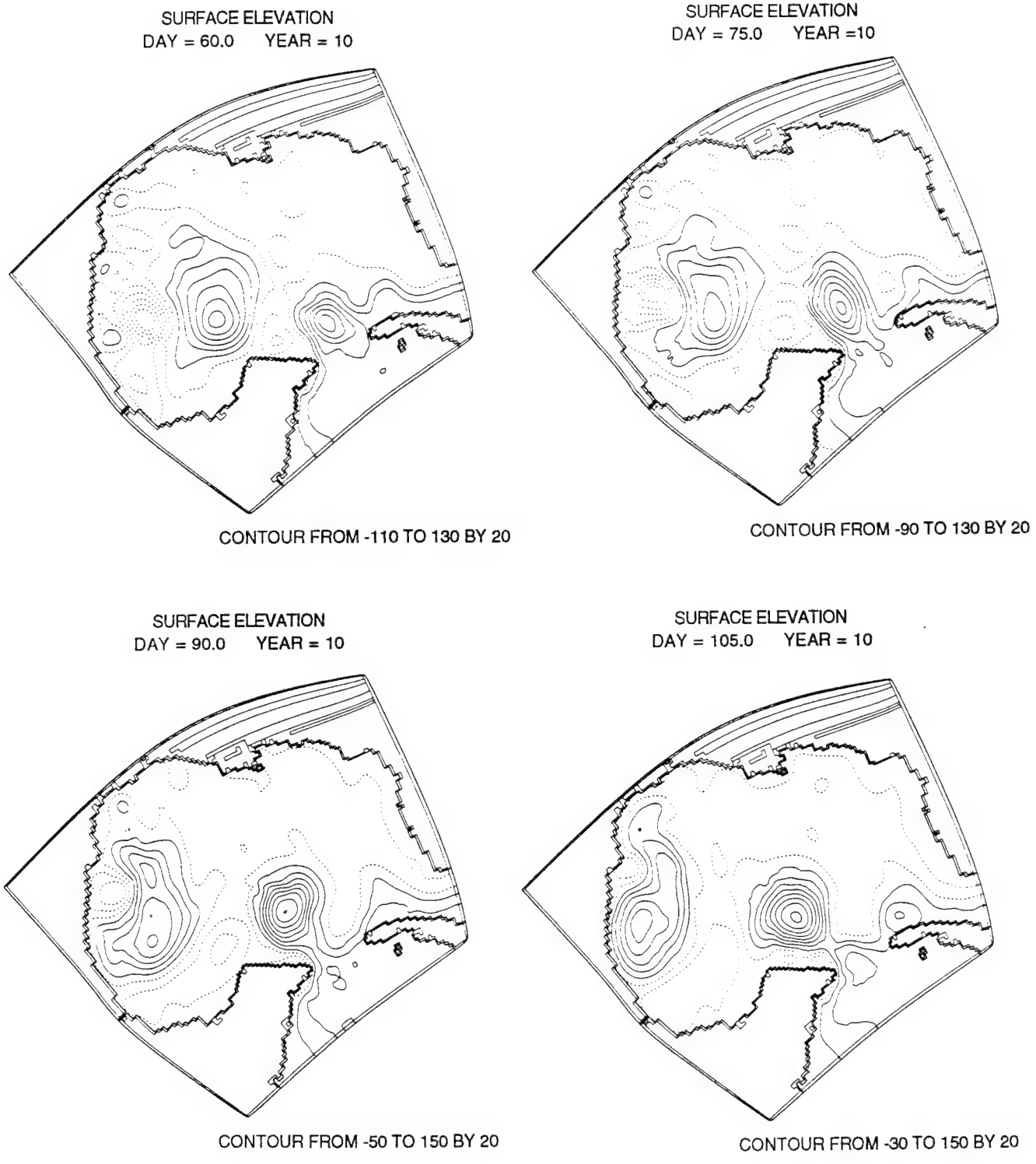

Fig. 4.2b : An eddy shedding event from GOM_2. (dt= 15 d), (dη=20 m).

GOM_3

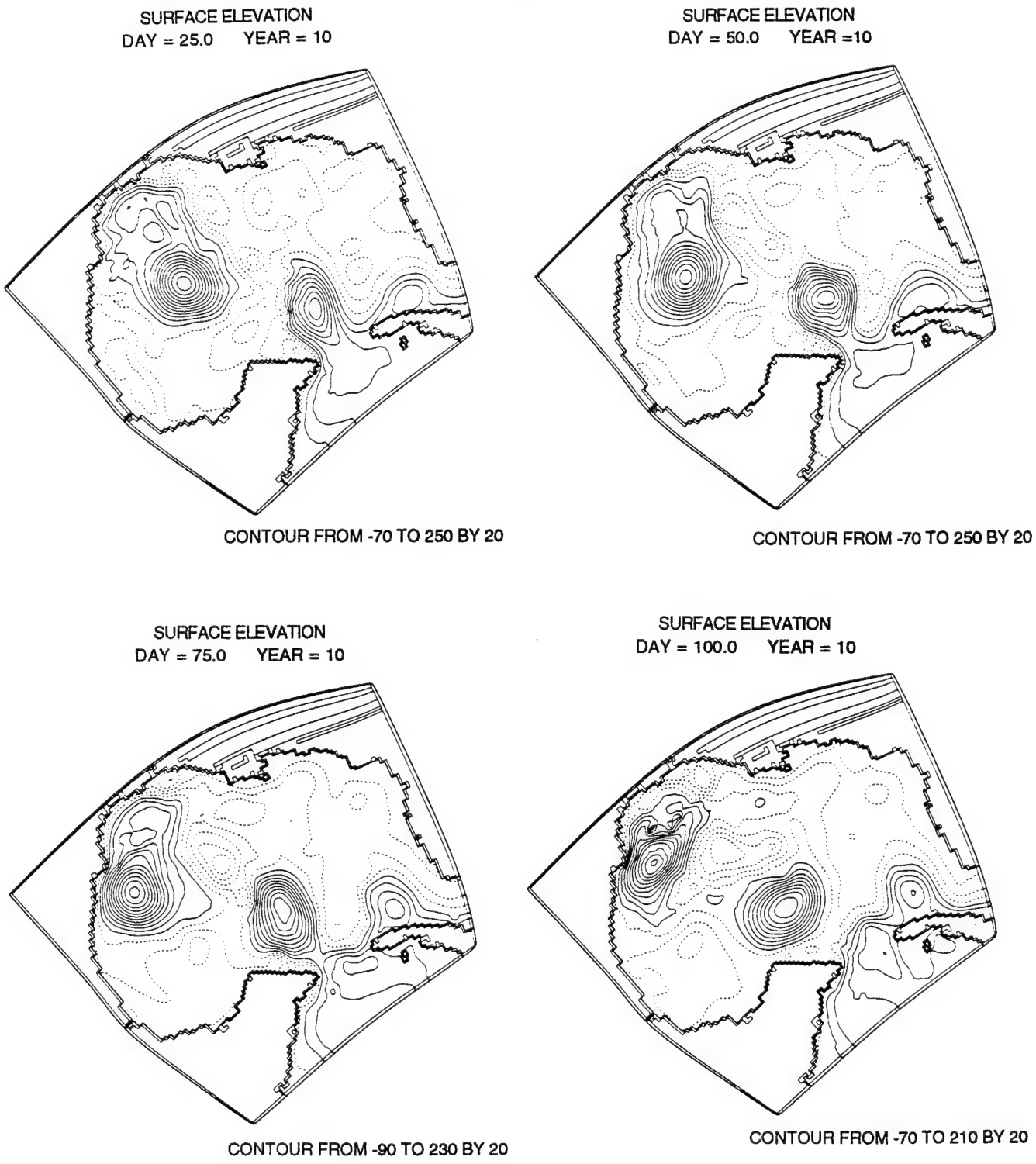

Fig. 4.2c : An eddy shedding event from GOM_3. (dt= 25 d), (dη=20 m).

GOM_4

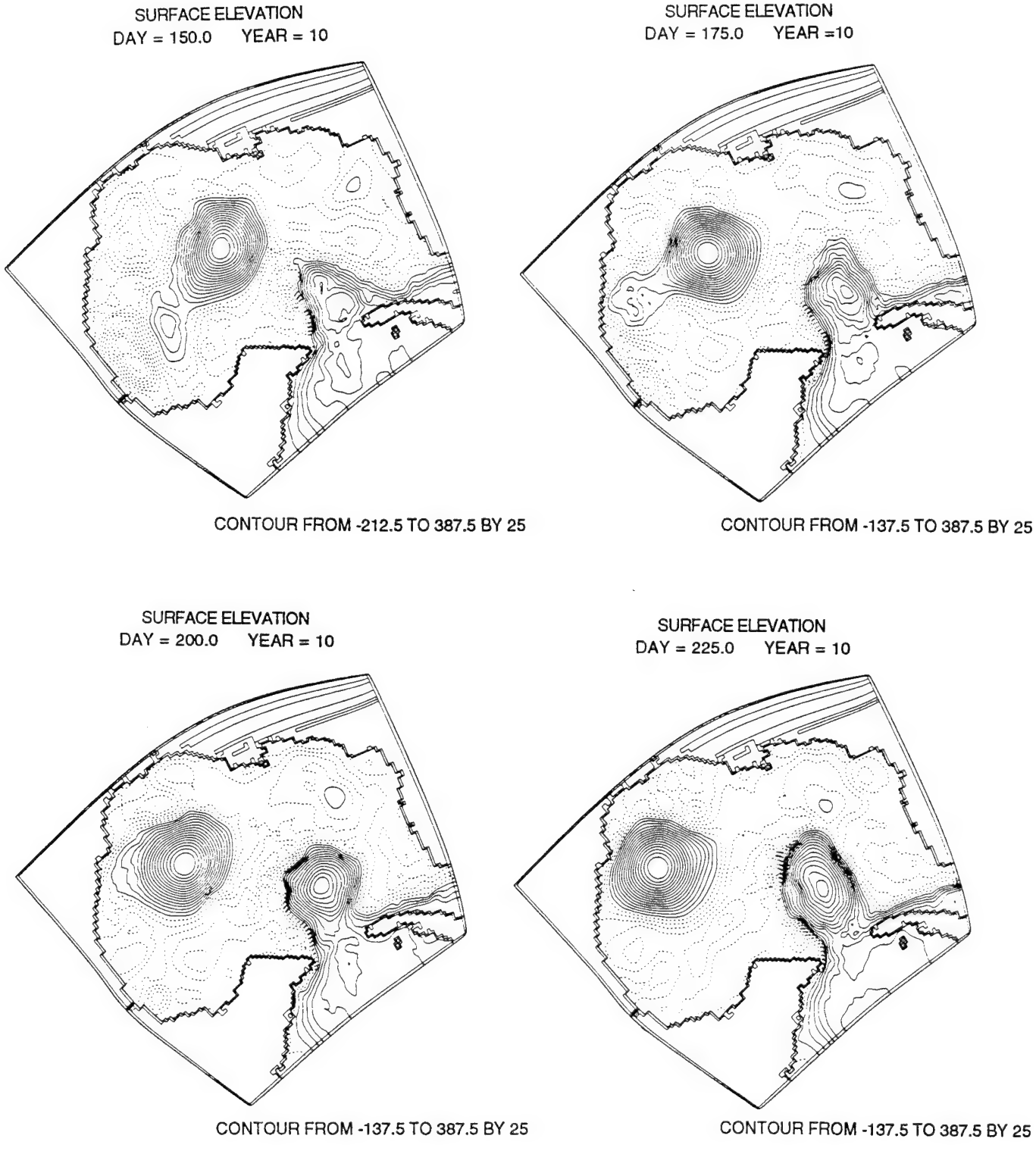

Fig. 4.2d : An eddy shedding event from GOM_4. (dt= 25 d), (dη=25 m).

GOM_4

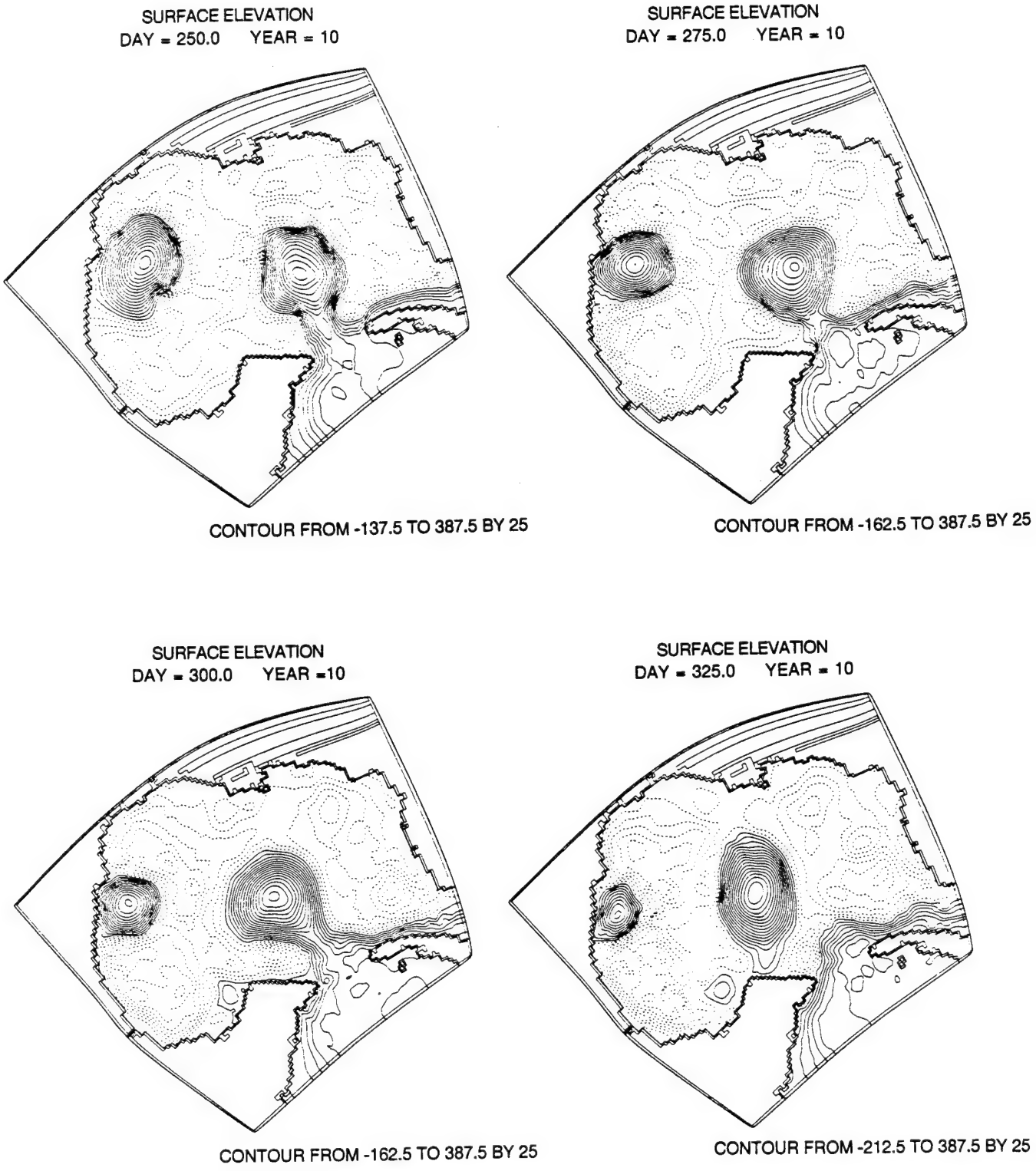

Fig. 4.2d Contd.

waves:

$$C_{Rw} = -\beta L_R^2$$
$$C_{Rwd} = C_{Rw} \frac{1}{1 + (\pi L_R / 2r)^2}, \tag{4.1a}$$

respectively. The theoretical values of the Rossby waves phase speed are summarized in Table 4.3. In the computations, the Coriolis parameter f_o=.72e-4 s^{-1} and the eddy radius of Table 4.2 have been used.

With respect to the Rossby wave propagation, GOM_1 and GOM_2 show reasonable agreement with the above phase speeds. More difficult is to relate the higher velocity values of GOM_3 and GOM_4 with HT linear theory. Nof (1983) considers the β-induced drift of an isolated nonlinear vortex and highlights the differences between cold and warm ring evolutions that are not known in the linear theory. Under the assumption that the radius, r, of the vortex is large compared to L_R, the nonlinear anticyclonic vortices migrate westward at a velocity:

$$C_a = C_{Rw} \frac{1 + \chi}{1 + \sqrt{1 - 8\chi(L_R/r)^2}} \tag{4.1b}$$

where $\chi = \eta/h$, and η the maximum surface displacement at the center of the eddy. The agreement between the theoretical estimates of Table 4.3 and the values calculated from GOM_3 and GOM_4 is remarkably good.

The migration velocity is drastically reduced when the eddy approaches the western boundary. When the center of the anticyclonic eddy is at a distance from the wall comparable with its own diamater, the paired cyclonic ring forms and the anticyclonic eddy is partially arrested. As the cyclonic gyre starts moving northward, the warm-core ring moves further westward, impinges the boundary and turns northward.

Fig. 4.3 illustrates the annual mean distribution of the upper layer anomaly. The amplitude of the EOF modes is illustrated in Fig. 4.4 and summarized in Table 4.4. Although the mean distribution is not representative of eddy shedding events, it illustrates the westward migration of the LpCur features. It follows that in GOM_1 and GOM_2 the LpCur disturbances are exceedingly tilted westward and move along the Yucatan coast. In GOM_4, the LpCur is more realistically oriented and extends in the central and eastern basin. The mean distributions do not make evident the presence of the cyclonic gyre at the Texas shelf (Fig. 4.2) because

SEA SURFACE DISPLACEMENT

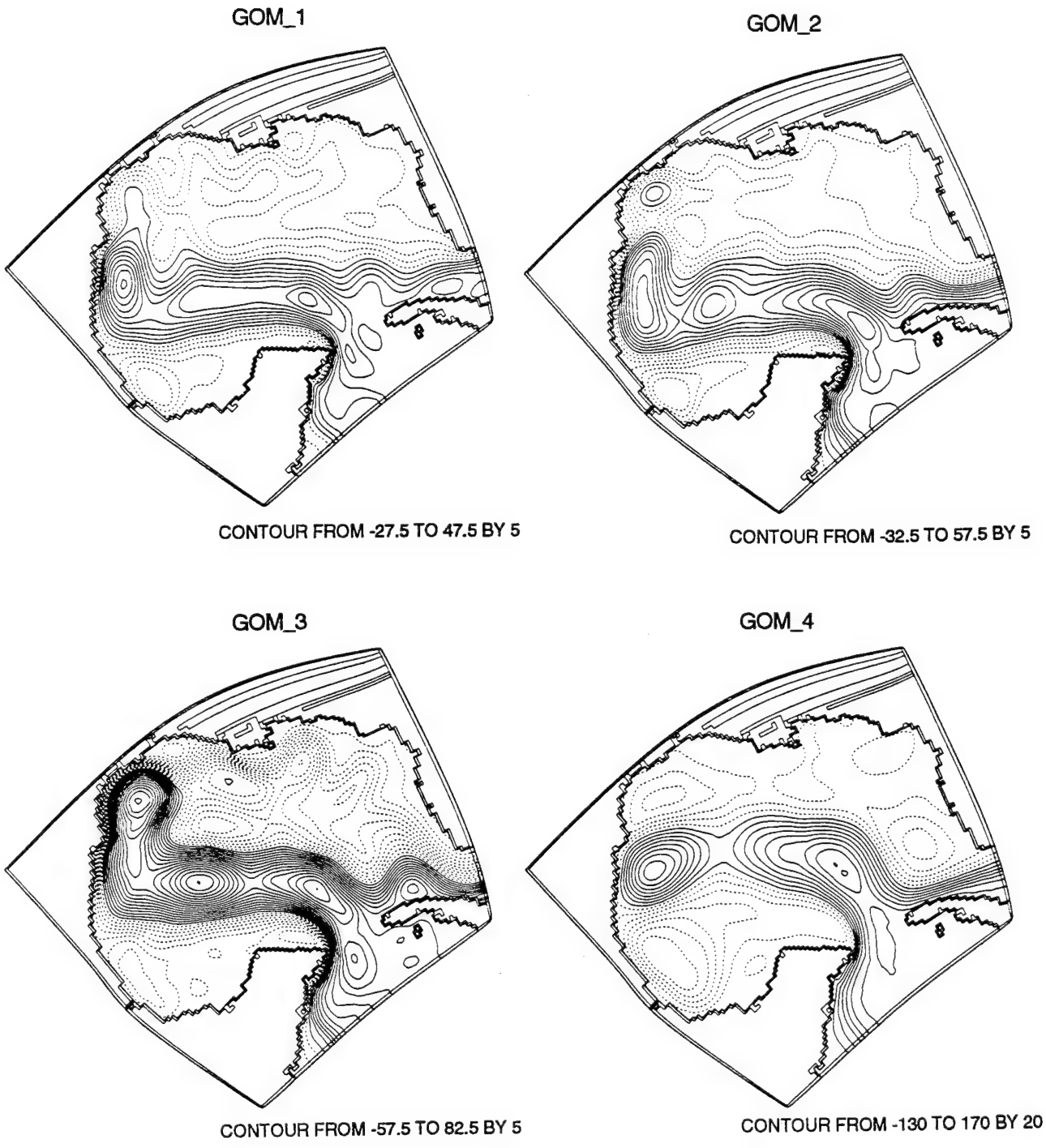

Fig. 4.3 : The annual mean of the sea surface displacement.

EOF MODE AMPLITUDE

GOM h 1250. sv =19.

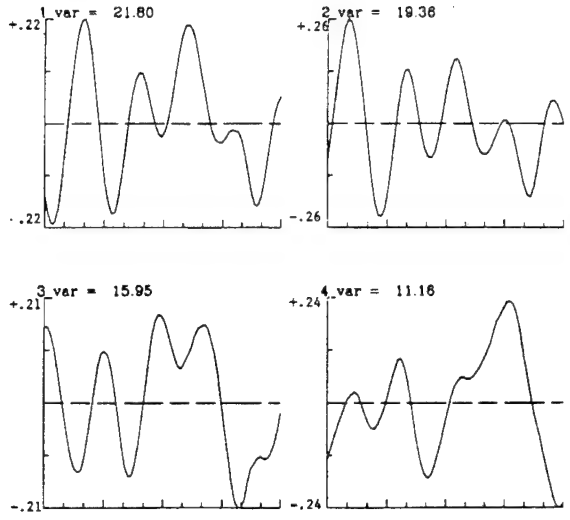

GOM h 1250. sv = 29.

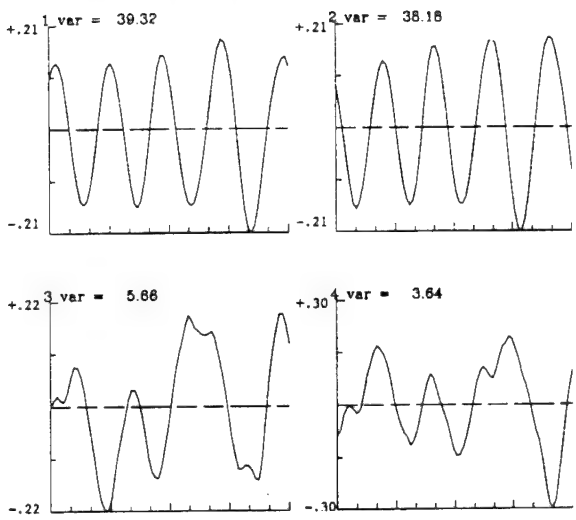

GOM h 450. sv = 14.9

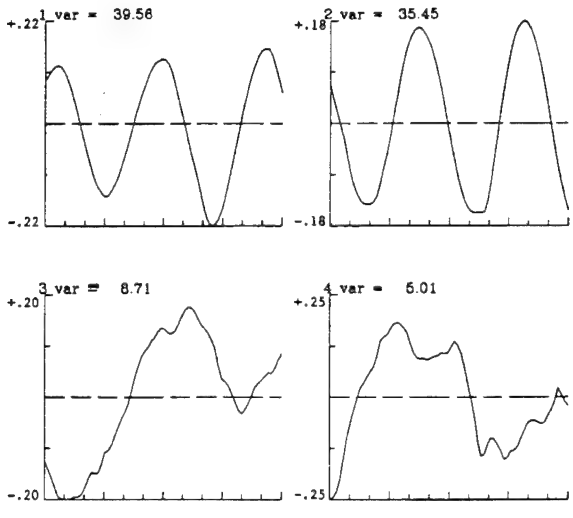

GOM h 450. sv = 31.

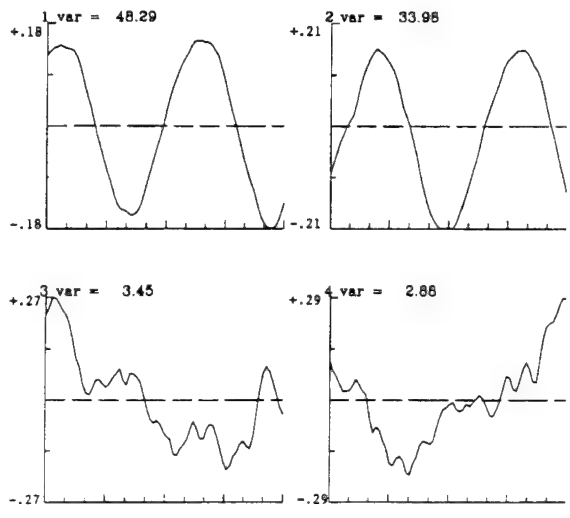

Fig. 4.4 : The deviation from the mean value of the EOF mode amplitude from the GOM experiments over a one-year cycle.

the anticyclonic features move northward with a path that often overlaps with that of the paired ring. Being less energetic than the anticyclonic features, the cyclonic ring is therefore removed from the mean distributions.

Table 4.3 The Theoretical Westward Translation Velocities

Experim.	C_{Rw}	C_{Rwd}	C_a
GOM_1	8.32	6.15	8.34
GOM_2	8.32	5.98	9.15
GOM_3	2.98	2.68	3.70
GOM_4	2.98	2.77	4.32

The theoretical translation velocities (km/day). See Eq. (4.1) for definition of terms.

The nonlinear character of GOM_4 is also made evident by the smaller- scale perturbations along the LpCur edges. Moreover, a cyclonic gyre develops between the eastern boundary of the LpCur and the Florida shelf before eddy separations. The cold Tortuga dome is well documented (Vukovich and Maul, 1985); tongues of cold water intruding into the warm LpCur off the Florida continental shelf have been observed by satellites. The tongues also show a clear cyclonic motion which stengthens before LpCur eddy separations.

The saddle point of the LpCur in GOM_3 is located west of the YucStr, north of Cuba. This configuration is due mainly to the specification of the OBC applied at the FlaStr which concentrates most of the outflow transport in the southern part of the port. Simulations in which the annual mean outflow is uniformly distributed across the strait, show a much less marked dome north of Cuba. In that case, the western edge of the *unperturbated* LpCur moves inside the central basin far from the western tip of Cuba, and the main stream assumes a smooth, U-reverse shape. In the other numerical experiments, the OBC produces an almost parabolic outflow velocity profile with the maximum speed in the central/southern part of the strait, so that the specification of uniform outflow transport does not sensibly alter the circulation inside the GOM. The maximum outflow transport of

GOM_4 is more located in the central part of the FlaStr, leaving an almost stagnant region north of Cuba.

Table 4.4 The Dominant Frequencies of the EOF Modes From the GOM Simulations

Experim.	Mode 1	Mode 2	Mode 3	Mode 4
GOM_1	75-140	80-160	230	185
GOM_2	85	85	110	175
GOM_3	160	155	360	285
GOM_4	210	210	185	360

The dominant periods (in days) of the EOF first modes from the GOM simulations. See Table 3.4 for definition of terms.

The annual cycle of the Fla outflow and the GOM transport anomaly are illustrated in Figs. 4.5 and 4.6, respectively. The experiments GOM_1 and GOM_2 are greatly affected by the specified nudging time scale of the OBC, so that the outflow is strongly constrained by the annual mean value, and the GOM anomaly is equivalent to the variance of the YucStr transport. The experiments GOM_3 and GOM_4 are less affected by the nudging time scale, and the outflow transports are consistent with the outcome of the NAtl simulations.

4.3 Sensitivity to Lateral Mixing

HT indicates, first, that eddy shedding of the LpCur occurs within a given range of the eddy viscosity values and identifies 4 regimes for the GOM variability. Highly diffusive simulations do not reproduce eddy separation but enhance the genesis of large meanders that may extend up to the western boundary. As the viscosity is decreased, there is a transition regime in which eddies may shed but stay confined inside large meanders. Further reduction of viscosity allows eddy shedding. In the ultimate inviscid case, the LpCur does not penetrate inside the GOM, but moves directly along the Cuban coast, little affecting the inner basin circulation.

Florida outflow

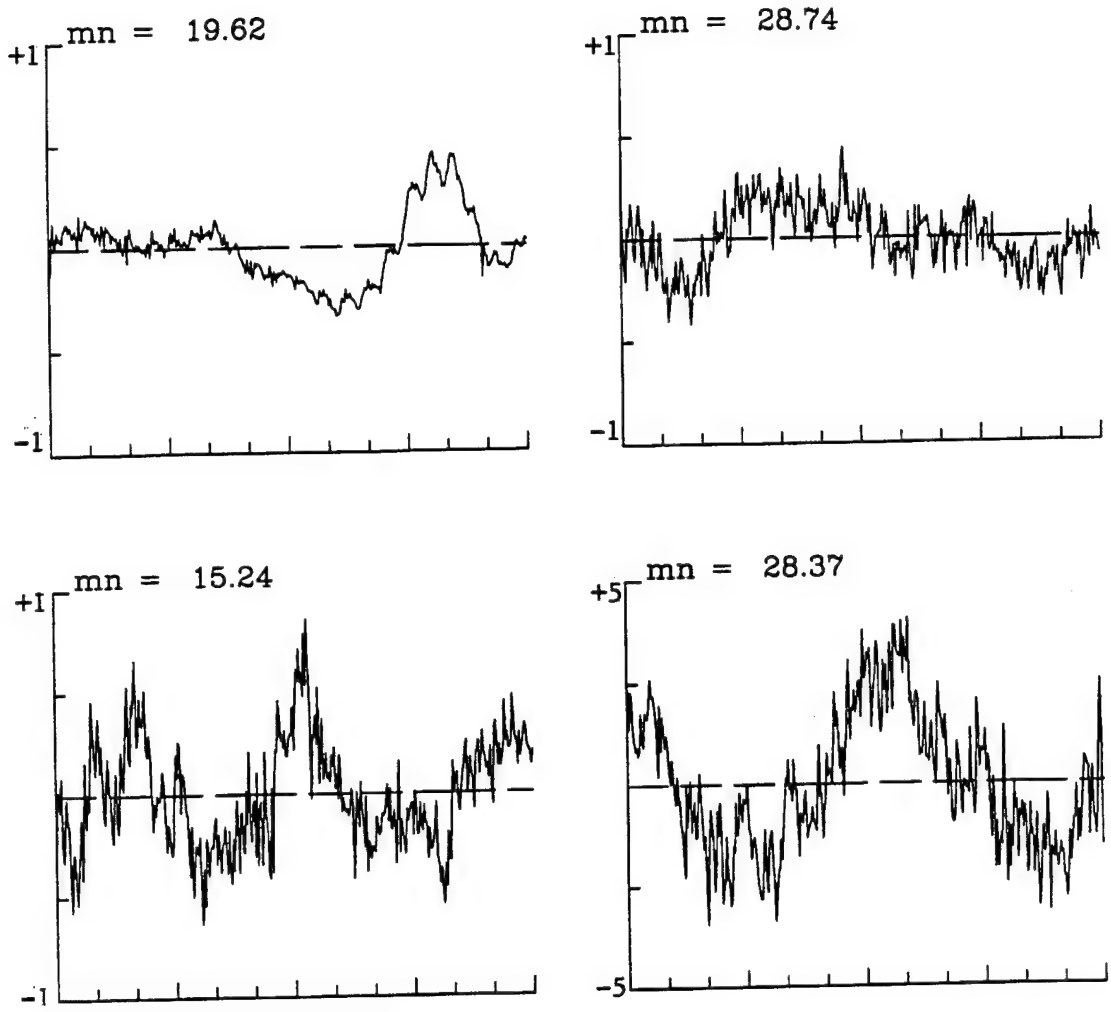

Fig. 4.5 : The annual transport at the FlaStr open boundary. Same as Fig. 3.6.

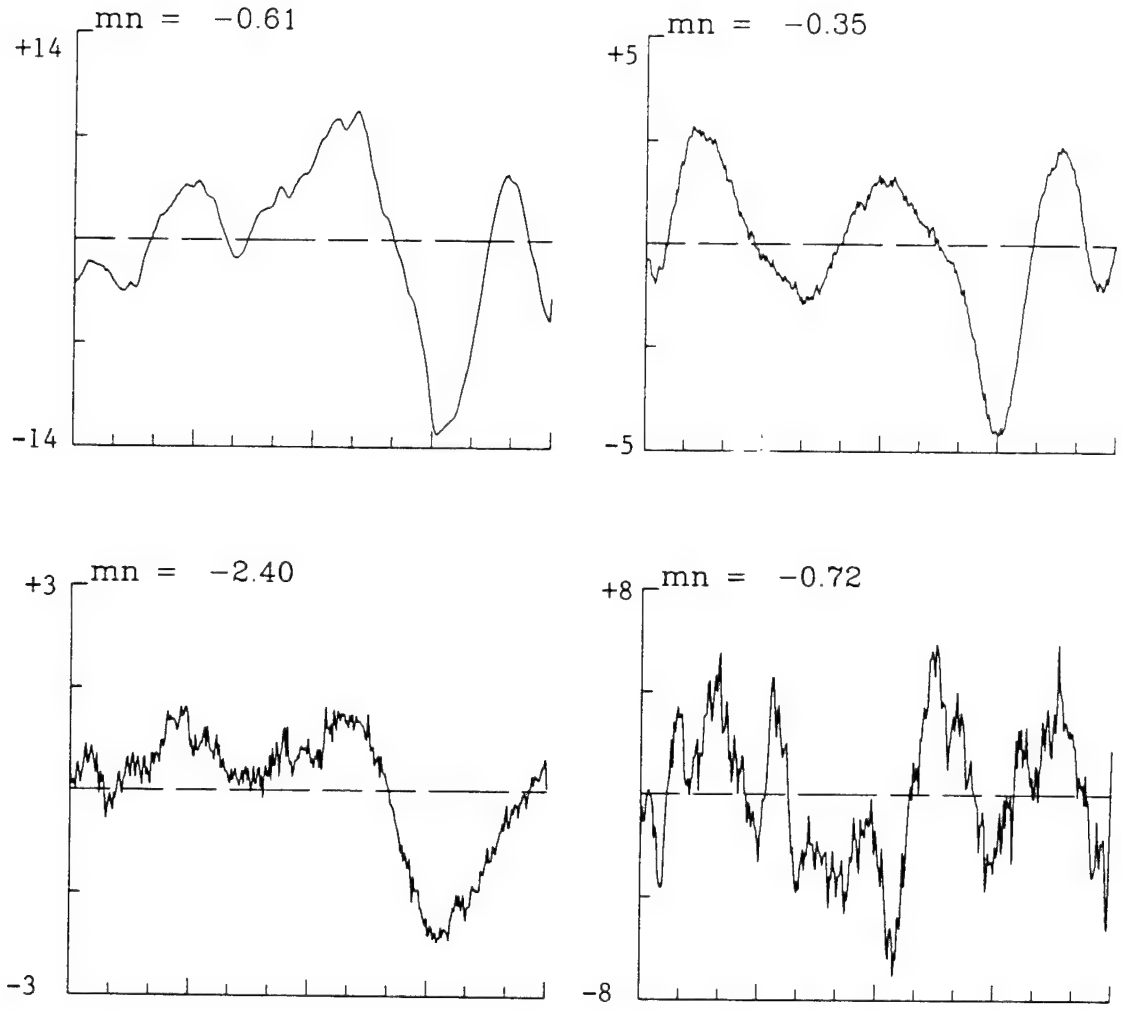

Fig. 4.6 : The GOM annual transport anomaly from the GOM experiments. Same as Fig. 3.6.

Additional tests, using several values of the lateral mixing coefficients, have been conducted in both NAtl and GOM configurations. Although the number of the simulations is insufficient for a detailed description of the LpCur regimes, the results may be summarized as follows:

- The annual mean wind-driven transports at the YucStr and WinPas (from the NAtl experiments) are independent of the lateral mixing. However, at high viscosity values, the standard deviation of the time series is sensibly reduced.
- Specification of the lateral mixing does not affect the time scale of the LpCur instabilities: for high viscosity coefficients, eddy shedding events are replaced by large meander formations that occur at the same frequency.
- The numerical experiments confirm HT results and identify the 4 regimes previously described. The range of the eddy viscosity coefficients in which the regimes are identifiied is a function of the Rossby radius and grid resolution.
- The size of the rings is proportional to the viscosity coefficients. As the lateral mixing is decreased, there is more evidence of small-scale variability that is generated south of the YucStr and carried inside the GOM by the main stream.

5. SUMMARY AND CONCLUSIONS

A reduced-gravity ocean model is configured in the NAtl Ocean and in the GOM to investigate the wind-driven circulation of the basin and the variability of the associated current systems. The analysis is focused on the circulation of the western tropical NAtl and its relationships with the dynamics inside the GOM. Several experiments verify the dependence of the solutions as functions of the Rossby radius of deformation (i.e., the thickness of the upper layer), and specification of the SAtl inflow.

Many aspects of the seasonal fluctuation of the NAtl depend upon Rossby waves. The EOF modal decomposition indicates that the eastern and central part of the basin is dominated by annual Rossby waves traveling across the domain at an approximate angle of 30^{o} with longitude. The western basin is dominated by the mesoscale variability associated with the western currents. Although locally highly energetic, the mesoscale variability accounts for no more than 25% of the first EOF mode total energy. Stammer and Boning (1992) propose a linear relationship between the first internal Rossby radius and the eddy length scale. In this respect, the NAtl experiments are broadly defined as eddy and non-eddy re-

solving simulations. It follows that the horizontal resolution alone is not sufficient to increase the level of kinetic energy (Beckmann et al., 1994), and no significant differences are found in the ratio between the eddy and mean flow kinetic energy for the two groups of experiments.

The geometry of the western tropical NAtl has a deep effect on the large scale circulation and Rossby waves propagation. Part of the subtropical gyre enters the CarSea through the several openings and straits between the Caribbean Islands; Rossby waves impinge the Central American coast and are reflected southward. Since the NAtl numerical domain does not include the Windward Islands, most of the reflected Rossby waves can leave the CarSea and rejoin the subtropical gyre. Because of this unrealistic configuration, the model requires higher values of the SAtl inflow to match the observed FlaStr transport. Indeed, the model includes the geometry of the WinPas, and the transport across the opening is consistent with estimates and observations.

The two flow components that enter the CarSea from the broad southern opening and the WinPas organize into a narrow western current north of the Nicaraguan coast. The YucCur supports mesoscale activity; eddies, with a length scale of approximately 50 km, are generated south of the YucStr and are carried inside the GOM.

The dynamics inside the GOM are analyzed with both the basin-wide NAtl and limited-area, high-resolution GOM models. Both configurations are able to reproduce eddy shedding. The time scale of the LpCur variability and the length scale of the rings does not depend upon the grid resolution of the NAtl and GOM domains.

The NAtl simulations, not affected by the specifications of the open boundary conditions, indicate that the transport at the YucStr and FlaStr are not strongly correlated. In general, the YucStr inflow has greater variation than the FlaStr outflow. The latter is more uniformly distributed in time, with fluctuations mainly related to the local wind forcing. No significant correlation is also found between eddy shedding events and the GOM volume anomaly.

The evolution of the LpCur instability is strongly dependent upon the Rossby radius of deformation rather than inflow transport values. For large, L_R, the LpCur

does not penetrate much inside the basin, and eddy shedding occurs just off the YucStr. The rings separate from the main stream with little interaction and migrate westward as dispersive linear Rossby waves. As L_R decreases, the frequency of the eddy separation and the radius of the rings increase and the GOM dynamics become more consistent with observations. The effects of nonlinearity also increase, and the detached eddies migrate westward as nonlinear, isolated vortices. The nonlinear character of the dynamics increases with the inflow transport and enhances more interaction between the anticyclonic rings and the LpCur during separation events.

In all the simulations, a cyclonic gyre appears off the Texas shelf when the anticyclonic eddies approach the western boundary. Due to the simplified physics of the reduced-gravity formulation, the paired ring is the response of the western basin to the changes of the local ambient vorticity. Of course, this does not preclude more complicated dynamics such as the upwelling of shelf/slope water to compensate the downwelling ahead of the warm-core ring as discussed in Dietrich and Lin (1994). On the other hand, the Tortuga cyclonic gyre is reproduced by Exp_4 only. The nonlinear regime that characterized the dynamics of Exp_4, allows the LpCur to penetrate more northward, delays eddy separation after the internal swirl is fully developed, and enhances the Fla shelf to adjust to the new local ambient vorticity.

With respect to other numerical studies of the GOM, this work confirms that the dynamics are mainly controlled by the first internal Rossby radius of deformation. Secondary features, such as the paired cyclonic gyre and the Tortuga cold dome, are due to the conservation of the ambient vorticity. The high domain resolution does not sensibly affect the quality of the solutions. The main difference between this and other studies is the time dependent specification of the inflow transport. It is well known that the variations of the YucStr inflow have no significant impact on describing the dominant mechanisms of the LpCur instabilities; however, it introduces a new factor, contributing to the modulation of the eddy separation events. Perhaps, the most important feature is the presence of small-scale variability that is generated south of the YucStr and is carried inside the GOM by the main stream. These eddies may be highly energetic (with respect to the main current) and may increase the nonlinear character of the LpCur variability.

Acknowledgments: This work was supported by the Office of Naval Research (under Grant # N00014-92-J-4112). The numerical sumulations were conducted at the NAVOCEANO Supercomputer, the CWES High Performance Computing Center, and the Mississippi Center for Supercomputing Research. The author wshes to thank Mr. D. Fox and Mr. J. Metzger of NRL-Code 7323 for providing the EOF program package, and the climatological wind data sets, respectively. Thanks are also due to Dr. K. Hedstrom at Rutgers University for the continuous assistance in assessing the SWEM code.

REFERENCES

Arakawa, A. and V.R. Lamb; 1977: Computational Design of the basic dynamical processes of the UCLA general circulation model. In *Methods of Computational Physics*, **17**, 14-265.

Beckmann, A., C.W. Boning, B. Brugge, and D. Stammer; 1994: On the generation and role of eddy variability in the central North Atlantic. *J. Geophys. Res.*, **99**, 20381-92.

Blumberg, A.F. and G.L. Mellor; 1985: A simulation of the circulation in the Gulf of Mexico. *Isr. J. Earth Sci.*, **34**, 122-44.

Brooks, D.A. and F.J. Kelly; 1986: The interaction of a Loop Current ring with the continental shelf in the western Gulf of Mexico. *Proceedings of the seventh annual Gulf of Mexico information transfer meeting.* New Orleans, LA, OCS Study/MMS Report 87-0058, 255-300.

Camarlengo, A.L. and J.J. O'Brien; 1980: Open boundary conditions in rotating fluid. *J. Comp. Physics*, **35**, 12-35.

Cooper, C., G.Z. Forrestal, and T.M. Joyce; 1990: Velocity and hydrographic structure of two Gulf of Mexico warm-core rings. *J. Geophys. Res.*, **95**, 1663-79.

Dietrich, D.E. and C.A. Lin; 1994: Numerical studies of eddy shedding in the Gulf of Mexico. *J. Geophys. Res.*, **99**, 7599-615.

Elliott, B.A.; 1979: Anticyclonic rings in the Gulf of Mexico. *J. Phys. Oceanogr.*, **12**, 1292-1309.

Hedstrom, K.S.; 1993: User's manual for a semi-spectral primitive equation ocean circulation model. Version 3. *Institute for Marine and Coastal Sciences Report #93-23.* Rutgers University.

Hellerman, S. and M. Rosenstein; 1983: Normal monthly wind stress over the world ocean with error estimates. *J. Phys. Oceanogr.*, **13**, 1093-1104.

Hurlburt, H.E. and J.D. Thompson; 1980: A numerical study of Loop Current intrusions and eddy shedding. *J. Phys. Oceanogr.*, **10**, 1611-51.

REPORT DOCUMENTATION PAGE

Form Approved
OMB No. 0704-0188

1. Agency Use Only *(Leave blank).*

2. Report Date. September 1995

3. Report Type and Dates Covered. Technical Report

4. Title and Subtitle.
COUPLING A BASIN-WIDE, COARSE-RESOLUTION NORTH ATLANTIC AND A REGIONAL, FINE-RESOLUTION GULF OF MEXICO MODEL

5. Funding Numbers.
Program Element No.
Project No.
Task No.
Accession No.

6. Author(s).
Germana Peggion

7. Performing Organization Name(s) and Address(es).
Center for Ocean & Atmospheric Modeling
The University of Southern Mississippi
Building 1103, Room 249
Stennis Space Center, MS 39529-5005

8. Performing Organization Report Number.
TR-1/96

9. Sponsoring/Monitoring Agency Name(s) and Address(es).
Office of Naval Research
Code 1513: RKL
Ballston Centre Tower One
800 North Quincy Street
Arlington, VA 22217-5660

10. Sponsoring/Monitoring Agency Report Number.

11. Supplementary Notes.
ONR Research Grant No. N00014-92-J-4112

12a. Distribution/Availability Statement.
Approved for public release; distribution is unlimited.

12b. Distribution Code.

13. Abstract *(Maximum 200 words).*
A reduced-gravity model is configured in the North Atlantic and Gulf of Mexico to investigate the wind-driven circulation and the variability of the associated current systems. The analysis is focused on the circulation of the western tropical NAtl and its relationship to the mesoscale activity inside the GOM. Several experiments investigate the solutions as a function of the Rossby radius of deformation and the specification of the South Atlantic inflow. The GOM dynamics are analyzed with both the basin-wide coarse-resolution and the regional high-resolution models. Both configurations are able to reproduce eddy shedding: the time and length scales of the Loop Current variability do not depend upon the grid resolution. The NAtl simulations indicate that the transport at the Yucatan and Florida Straits are not strongly correlated. Also, no significant correlation is found between eddy shedding events and the GOM transport anomaly.

14. Subject Terms.
(U) NORTH ATLANTIC, (U) GULF OF MEXICO, (U) EDDY-RESOLVING MODELS, (U) REDUCED-GRAVITY MODEL

15. Number of Pages. 48

16. Price Code.

17. Security Classification of Report.	18. Security Classification of This Page.	19. Security Classification of Abstract.	20. Limitation of Abstract.
Unclassified	Unclassified	Unclassified	SAR